AD-A139 179 FUNDAMENTAL STUDIES OF GROWTH DOPING AND TRANSFORMATION 1/1
IN BETA SILICON C..(U) NORTH CAROLINA STATE UNIV
RALEIGH DEPT OF MATERIALS ENGINEERI.. R F DAVIS
UNCLASSIFIED 31 AUG 83 NCSU-243-043-003 N00014-79-C-0121 F/G 20/2 NL

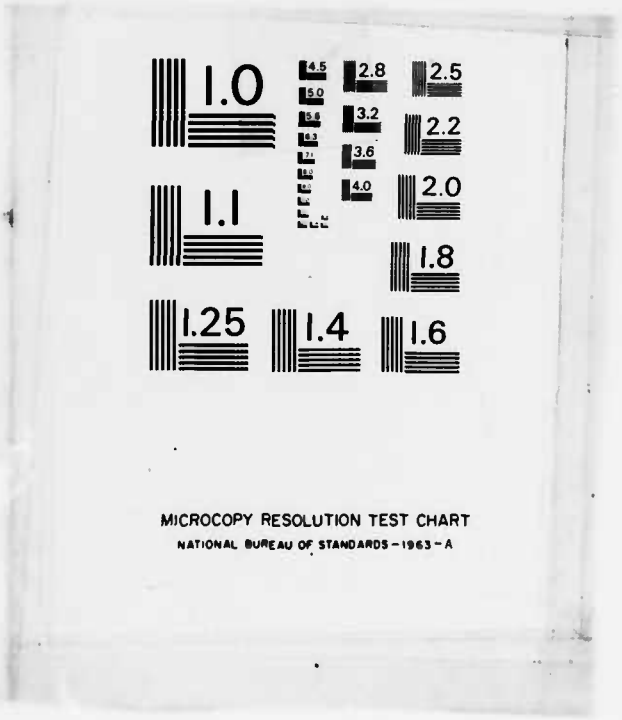

(14)

Annual Technical Report

on

FUNDAMENTAL STUDIES OF GROWTH, DOPING AND TRANSFORMATION IN BETA SILICON CARBIDE

Supported by ONR Under Contract N00014-82-K-0182

For the Period September 1, 1982 - August 31, 1983

School of Engineering

North Carolina State University

Raleigh, North Carolina

(14)

Annual Technical Report

on

FUNDAMENTAL STUDIES OF GROWTH, DOPING AND TRANSFORMATION IN BETA SILICON CARBIDE

Supported by ONR Under Contract N00014-82-K-0182

For the Period September 1, 1982 - August 31, 1983

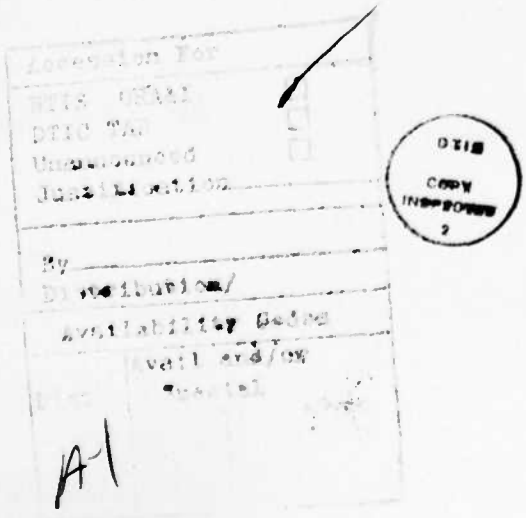

SECURITY CLASSIFICATION OF THIS PAGE (When Data Entered)

REPORT DOCUMENTATION PAGE

READ INSTRUCTIONS BEFORE COMPLETING FORM

1. REPORT NUMBER: 243-043-003	2. GOVT ACCESSION NO.: A139179
3. RECIPIENT'S CATALOG NUMBER:	
4. TITLE (and Subtitle): Fundamental Studies of Growth, Doping and Transformation in Beta Silicon Carbide	5. TYPE OF REPORT & PERIOD COVERED: Annual Report
	6. PERFORMING ORG. REPORT NUMBER:
7. AUTHOR(s): Robert F. Davis H. H. Stadelmaier	8. CONTRACT OR GRANT NUMBER(s): N00014-79-C-0121
9. PERFORMING ORGANIZATION NAME AND ADDRESS	10. PROGRAM ELEMENT, PROJECT, TASK AREA & WORK UNIT NUMBERS: PE 61153N RR 021-02-03 NR 243-027
11. CONTROLLING OFFICE NAME AND ADDRESS: ONR-427 Arlington, VA 22217	12. REPORT DATE:
	13. NUMBER OF PAGES: 54
14. MONITORING AGENCY NAME & ADDRESS (if different from Controlling Office): North Carolina State University Department of Materials Engineering 229 Riddick Laboratories Raleigh, NC 27695	15. SECURITY CLASS. (of this report): Unclassified
	15a. DECLASSIFICATION/DOWNGRADING SCHEDULE:

16. DISTRIBUTION STATEMENT (of this Report)

Approved for public release; distribution unlimited

17. DISTRIBUTION STATEMENT (of the abstract entered in Block 20, if different from Report)

Beta

18. SUPPLEMENTARY NOTES

ONR Scientific Officer; Tel: (202) 696-4218

19. KEY WORDS (Continue on reverse side if necessary and identify by block number)

Silicon Carbide	Ion Implantation	Ion microprobe
	Annealing	Converted Layer
Vapor Phase Epitaxy	n-type dopants	XPS
Thin Film	p-type dopants	Plasmon

20. ABSTRACT (Continue on reverse side if necessary and identify by block number)

Semiconductor quality β-SiC thin films are currently being grown for future microelectric applications using CVD techniques. Research in this period has included initial ion implantation studies coupled with annealing and ion microprobe analyses of the resulting implant profiles. An indepth study of the converted layer formed by the reaction of C_2H_4 with the Si substrate is also included in this report.

DD FORM 1 JAN 73 1473 EDITION OF 1 NOV 68 IS OBSOLETE
S/N 0102-014-6601

Enclosure (1)

SECURITY CLASSIFICATION OF THIS PAGE (When Data Entered)

I. Introduction

Silicon carbide is the only compound species that exists in the solid state in the Si-C system and can occur in the cubic (C), hexagonal (H) or rhombohedral (R) structures. It is also classified as existing in the beta and alpha modifications. The beta, or cubic, form crystallizes in the zincblende or sphalerite structure; whereas, a large number (approximately 140) of the alpha occur in the hexagonal or rhombohedral forms known as polytypes.

Because of the emerging need for high temperature, high frequency and high power electric devices, blue L.E.D.'s, Schottky diodes, U.V. radiation detectors, high temperature photocells and heterojunction devices, silicon carbide is being examined throughout the world for employment as a candidate material in these specialized applications. The electron Hall mobility of high purity undoped β-SiC is approximately a factor of three larger ($\sim$1000 cm^2/V-sec) than that of the α-form over the temperature range of 300-1000K because of the smaller amount of phonon scattering in the cubic material. The energy gap is also less in the β-form (2.3 eV) compared to the α-form (e.g., 6H = 2.86 eV). Thus, the β-form is now considered more desirable for electronic device applications. Therefore, the growth and characterization of semiconductor quality thin films of this material and their continual refinement has constituted one of the principal objectives of this research program. Unfortunately, the earlier push in the 1956-1970 time span to develop SiC as an electronic material concentrated heavily on high temperature growth processes such as the Lely sublimation-condensation technique which produced a variety of α polytypes in experiments which were rarely reproducible. Toward the end of this initial thrust, techniques such as chemical vapor deposition (CVD), sputtering, traveling solvent and solution growth showed promise not only as techniques *per se* but as experimental avenues wherein the growth of β-SiC could be achieved.

Under the previous grant, a method for the growth of single crystal thin films of β-SiC on (100) Si was developed using specially designed and very closely controlled variable pressure equipment and a two-step process. This method entails the initial chemical conversion of the Si

surface via a high temperature reaction with ethylene (C_2H_4). This step is followed by direct and continual deposition of β-SiC via the separate decomposition of SiH_4 and C_2H_4 on the converted layer. H_2 is the carrier gas in both processes. Computer-assisted calculations of CVD phase diagrams based on the process of free-energy minimization of thermodynamic data in Si-C-H system were also conducted in the previous program in order to discern the effect of the Si/Si+C ratio, H_2 partial pressure, total pressure and temperature on the size of the β-SiC phase field. These diagrams provided considerable guidance for choosing the parameters of deposition for the β-SiC films.

The specific objectives of the present research program include the expansion of the prior CVD effort to include (1) refinement of the growth technique in order to fabricate reproducible films in terms of surface quality and electronic properties, (2) the in-situ introduction and ion implantation of n- and p- type dopants, (3) electronic, structural, chemical and microstructural characterization of these films in order that (4) simple devices can be produced, (5) the determination of the effects of impurities on the β - α SiC transformation and its thermodynamic reversibility and (6) the growth of single crystals of β-SiC.

In addition to coordinating the above efforts, the Principal Investigator has spent a considerable amount of time during this reporting period in the development and installation of a CAMECA ion microprobe and its associated sample preparation laboratory. In addition, considerable time has been contributed to the "shakedown" period in order to correct problems resulting from both original manufacture and shipping and the incorporation of (a) new computer software and more recently (b) digital imaging of the chemical "map" of the sample. The Principal Investigator has also hired a Ph.D. in analytical chemistry to operate this instrument. The ion microprobe has proved invaluable in this research program for the understanding of the chemically converted layer initially grown on the Si surface prior to the deposition of a β-SiC thin film, as well as the determination of the ion implanted profiles.

The results accomplished during this reporting period as well as the objectives for the coming year are described below.

II. Program Review for 1982

A. Personnel

As all the graduate research personnel associated with the prior ONR research program received their respective degrees just prior to the January 31, 1982 termination date and as the Principal Investigator was on sabbatical leave to Japan during the last five months of this grant, the remainder of 1982 and a portion of 1983 were periods of recruitment of suitable post doctorates and graduate students for the new program. In the case of the former, a rather long waiting period was necessary in order for dissertations of the best candidates to be completed. However, the several years of cumulative theoretical and experimental knowledge and skills in high resolution electron microscopy, electronics and X-ray diffraction which these persons have brought to the program have been invaluable in the characterization of the ion implanted samples and the development of the program concerned with the causes and mechanism(s) of (1) the β - α SiC transformation and (2) the formation of polytism and stacking faults in this material. Graduate students (all Ph.D. candidates) with suitable backgrounds for this research program have also come on board throughout the latter part of 1982. Very recently, I have also added a Ph.D. student having one of the prestigious ONR Fellowships to coordinate and conduct a portion of the ongoing ion implantation and annealing effort as well as the initiation and conduct of the task concerned with the fabrication of simple devices in the SiC thin films. All but one has a research background in electronic materials. At this point, all positions are now staffed and the program is making progress in all areas.

B. Chemical Vapor Deposition of β-SiC Thin Films

The principal objectives of this aspect of the program include the reproducible growth of semiconductor quality β-SiC thin films on Si by CVD, the development and employment of techniques of in-situ incorporation of electronically active dopants and the determination of the effects of these dopants and their increasing concentration on the creation of stacking faults and the β - α SiC transformation. The first two aspects have been pursued during the past year, as briefly described below.

1. CVD System Modifications

A schematic of the CVD system modified at the beginning of this reporting period is shown in Fig. 1. Major portions of it have remained the same as that described in detail in a previous ONR document (See Annual Report #243-027-009 [for the period 1 Jan. '80 - 31 Dec. '80] for ONR Grant #N00014-79-C-0121); thus, a description of these areas will not be presented in this report. The newly added or modified portions are shown within the dashed lines; only those aspects will be described here.

The new gas lines will be used to carry the electronically active dopants of N_2 and P (n-type) and Al and B (p-type). Each type of dopant has a separate line containing the same elements of check valve, flowmeter, flow control value and line shut-off valve as are present in the reactant and carrier gas lines of SiH_4, C_2H_4 and H_2.

In private communication with several research persons throughout the world who are or who have worked with SiC, it was learned that B appears to occupy both the C and the Si sites (although from a consideration of covalent sizes alone, the occupation of the C site would seem most favorable) as a function of B concentration (and probably temperature). The incorporation of this element is also believed to catalize the β - α SiC transformation. For these reasons, Al has been chosen as the initial p-type dopant.

Both the n-type and p-type lines are now in place. The p-type line required special configuration, as the chosen source is trimethylaluminum [$Al(CH_3)$] with H_2 as the diluent and carrier gas. As the vapor pressure of this liquid phase material must be closely controlled, precise control of temperature must also be maintained. To this end, a special dewar and constant ($\pm 0.1°C$) temperature bath have been fabricated and purchased, respectively, for this purpose.

Each of the dopant gas lines has a gas-collection bottle (part Y in Fig. 1) which can be detached from the line and attached directly to a gas chromatograph mass spectrometer in order to analyze the concentration of the dopant in the line.

The external part of the reactor chamber has also been almost completely modified in order to achieve both more efficient cooling and

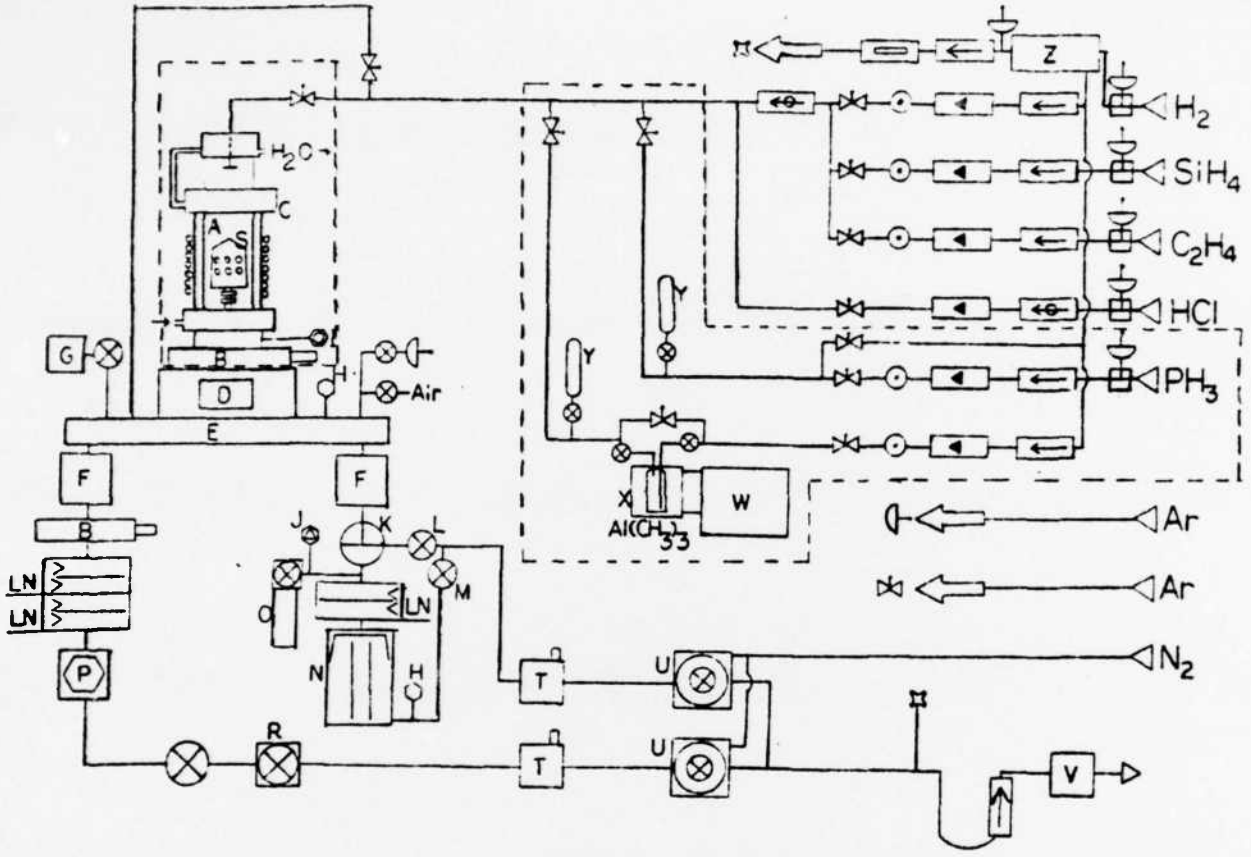

Figure 1. Schematic of NCSU chemical vapor deposition equipment for the growth of β-SiC thin films. Dashed lines denote recently installed portions, as described in the text. Symbols are defined on the following page.

Nomenclature for Symbols on Figure 1.

A. RF-heated CVD reaction chamber
B. Automatic valve to chamber
C. Water cooling jacket
D. Door for loading chamber
E. Stainless steel chamber
F. Particle trap
G. Baratron pressure sensor
H. Thermocouple vacuum gage
I. Convectron vacuum gage
J. Ionization vacuum gage
K. Manual gate valve
L. Roughing valve
M. Foreline valve
N. Diffusion pump
O. Residual gas analyzer chamber
P. Liquid collection chamber
R. Automatic butterfly valve
S. Substrates and susceptor
T. Molecular shieve trap
U. Mechanical pump
V. Bunsen burner
W. Refrigerated circulating bath
X. Cooling bath for $Al(CH_3)_3$ bottle
Y. Sampling bottle
Z. Hydrogen purifier

the ability to vary the distance between the reactant gas entry tube and the SiC-coated graphite susceptor (and thus the Si wafers). Several susceptors of different shapes and sizes have also been designed and employed in order to determine the optimum configuration for the growth of the best films.

Concerning this last point, because of differences in thickness of the β-SiC films grown in the top portion of the susceptor relative to those in the middle of the susceptor and the formation of an undesirable amount of SiC on the top of the susceptor, several design changes were made, particularly in the length and taper of the very top of this most important item of the reactor system. The final result is both a lengthened susceptor wherein the very top portion sticks out of the r-f coil in order to more gradually heat and control the dynamics of the flow of the incoming gas stream and a modified entry port on the gas inlet tube so that the gas does not directly impinge on the top cone of the susceptor.

Finally, a residual gas analyzer has been connected to the system in order to determine the presence of impurities in the reactant and dopant gases as well as absorbed gases in the chamber, and a larger H_2 purifier has been placed in operation in order to allow higher flow rates of this gas.

2. Growth of β-SiC Thin Films

The graduate student assigned to the CVD system has now learned to produce films of even higher microstructural quality on 1-cm extrinsic ($\rho \geq 10$ kohm-cm) and intrinsic (100) Si than fabricated in the previous program. A large number of runs have been made wherein the films contained zero fringes and the final surfaces were suitable for integrated circuit fabrication. Samples have been and continue to be supplied to the students conducting the ion implantation and annealing research and will be used for oxidation studies when all the new equipment has been received and installed and some of the existing equipment repaired. Samples have also been supplied to the Naval Research Laboratory, Lockheed Research Laboratory, The California Institute of Technology and to Cornell University for evaluation and characterization.

In the initial months of this year, some research time was devoted to not only the determination of the optimum chamber, susceptor and inlet tube configurations but also to varying the deposition conditions to determine the optimum CVD conditions for the growth of semiconductor quality films. The initial work was all conducted at one atmosphere; however, it has been found that lowering the pressure slightly to 380 torr produces a much smoother surface but a lower growth rate. Increasing the line flow rate of H_2 to 4000 sccm (at one atmosphere pressure) with accompanying flow rates of SiH_4 and C_2H_4 of 2 sccm and 1 sccm, respectively, also produces a smoother surface than with H_2 flow at 3000 sccm without a reduction in growth rate.

Equipment for angle lapping and the techniques necessary to employ this process for the determination of the thickness of the various films have been completed during this reporting period.

3. Residual Gas Analysis

The installation and employment of the RGA noted above has proved invaluable in (a) evaluating the system for leaks and (b) detecting the presence of impurities in the various gases and chamber. One example of its use was the determination of the presence of N_2 in the C_2H_4 bottle which considerably exceeded the manufacturer's specifications. This and the SiH_4 have been replaced; the latter because of purer material now available on the market. Although this has notably improved the quality of the input reactant gases, some residual N_2 apparently remains in the system. One indication of this is the much higher resistivity of the samples which have been grown in the chamber after it has been pumped to 10^{-6} Torr compared to those grown after the chamber has been mechanically pumped and purged three times with argon. In addition, it was very recently learned, in chance conversation with persons directly involved in the SiC coating of our susceptors, that N_2 is used as the carrier gas for the methyldichlorosilane from which the SiC coating is produced. Arrangements are now being made to substitute H_2. If this is not successful, we shall coat them in our own reactor, even though two-three days are required for each susceptor. Finally, we have instituted a monthly vacuum leak-check operation of the entire system. This has proven very valuable in reducing the concentration of electronically active species as well as oxygen and has allowed us to produce a better surface on the as-grown films.

C. Ion Implantation, Annealing and Ion Microprobe Analysis

1. Introduction

Since (1) the β-SiC films are grown on and remain on Si which has a melting point of 1683K, (2) the mass transport rates of electronically active dopants such as B, P, Al and N, are very slow in SiC even at 2273K and (3) Si begins to very slowly sublime from SiC above 1873K, it appears unlikely that dopants can be incorporated into SiC by diffusional processes commonly used in the semiconductor industry. Thus, in-situ doping of the aforementioned elements during growth for the fabrication of discrete devices and ion implantation for device structures useful for both discrete devices and integrated circuits appear to be the most viable routes. Our effort within this report period, concerning the ion implantation of these species, the subsequent annealing and the characterization of the implanted and annealed profiles is presented below.

2. Ion Implantation

The dual objectives of ongoing ion implantation study have been (1) to produce standards which can be used to (a) compare with the theoretical LSS calculations for the position and concentration value of the peak concentration and to (b) determine the concentrations of the various dopants introduced via the CVD and subsequent ion implantation studies; and (2) produce samples containing dopants at device concentration levels which can be used for the damage annealing studies described below.

Since essentially nothing is known concerning ion implantation and damage recovery in β-SiC,* it has been imperative to determine the position of the implant peak maximum and compare this with the theoretical LSS calculations. Secondary ion mass spectrometry depth probing has been conducted using the CAMECA ion microprobe noted in the introduction coupled with surface profilometry to determine the shape of the implanted profiles and the rate of sputtering (i.e. profiling) of the ion probe,

---

* The LSS calculations exist for various dopants in SiC; however, one cannot determine if a cubic β-SiC or one of the hexagonal or rhombic polytype structures was considered in calculating the data.

respectively. Once the rate of sputtering is known, the actual position of the peak maximum for each dopant can be determined and compared with the LSS calculated value. Examples of this, drawn from our many implant experiments at room temperature, are shown in Figures 2, 3 and 4, for B, N and P, respectively (Al standard implants will be produced in the near future). In these figures, the actual implant is shown as the solid line while the theoretical LSS calculation is presented as a broken line. The experimental conditions used to make these three implants and to determine the profiles are given in Tables I and II.

It is important to determine the position of the implanted peak relative to the theoretical position for each of the elements noted above under different ion implantation conditions which would be used to produce devices in order that decisions can be made concerning the formation of implanted junctions using different n-type (N and P) and p-type (Al and B) elements. Furthermore, one cannot accurately evaluate the total concentration of the dopant species produced in the in-situ doped material or any changes in this concentration as a function of depth in the thin film without direct chemical comparison with the ion implanted standards. The capacitance-voltage measurements that we have been able to make provide a calculated charge carrier concentration, but not the percent activation of the total dopant concentration.

In every B and N implant profile examined, the actual <u>position</u> of the peak maximum occurred at a slightly more shallow depth than the calculated value, as may be seen in Figures 2 and 3. For the P implants (see Fig. 4), however, the theoretical and actual peak positions are essentially identical. In addition, the peak <u>concentration</u> of each implanted species compared very well with the calculated value for all the implants thus far investigated. The distances shown on the abscissas of these graphs (and, therefore, the position of each of the implant peaks) were determined by angstrometer measurements of the depths of several broad valley craters produced by the ion microprobe using the same primary ion current for increasing lengths of time. Knowing this calculated rate of depth probing coupled with the continued use of the same primary ion current for each implanted species, we can precisely

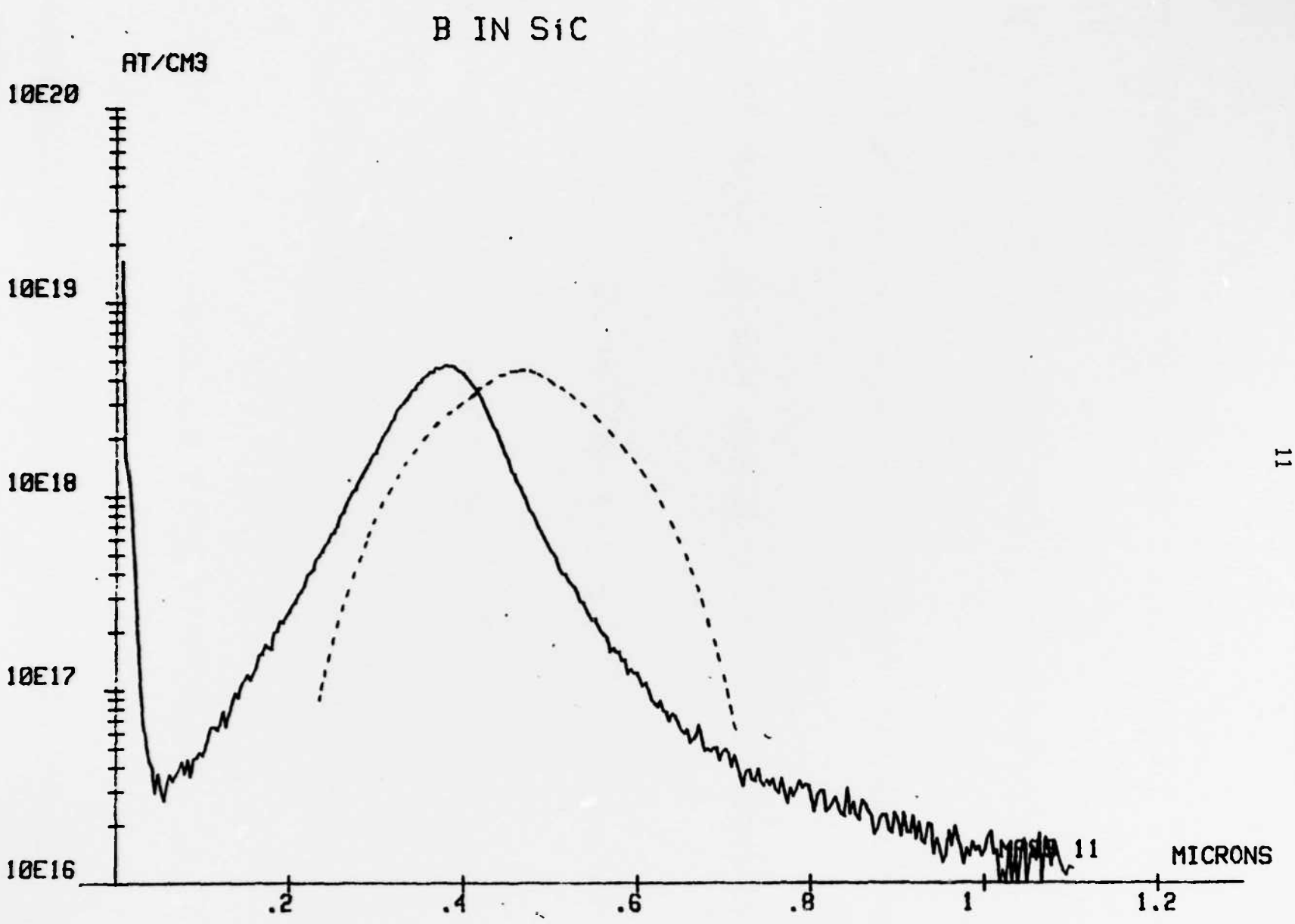

Figure 2. SIMS depth profile (solid line) of B implanted into in β-SiC at 200 keV, $7.6 \times 10^{-13}/cm^2$ and room temperature. Broken line is the Gaussion distribution calculated from LSS theory.

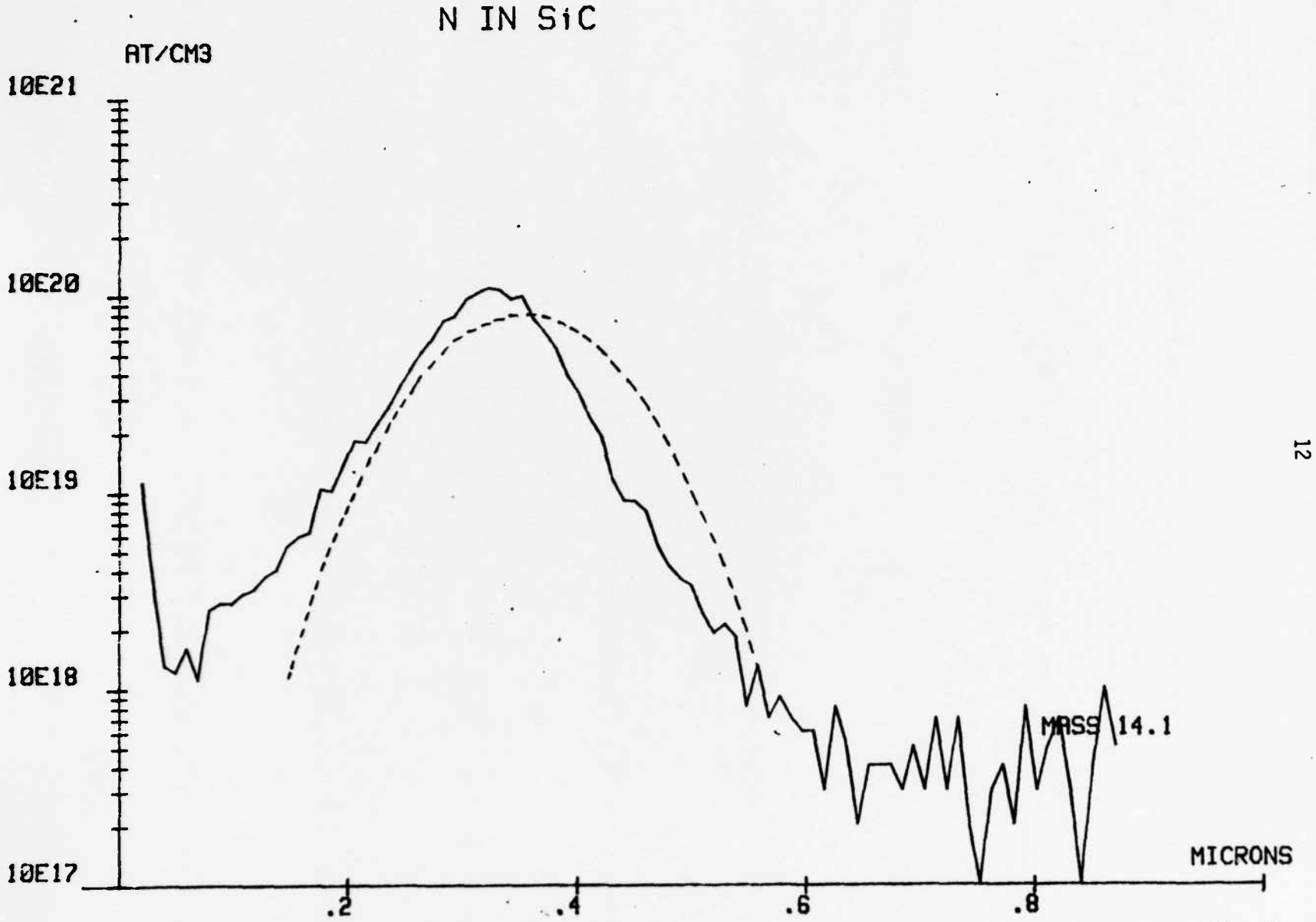

Figure 3. SIMS depth profile (solid line) of N implanted into β-SiC at 200 KeV, 1.5 x 10^{15}/cm^2 and room temperature. Broken line is the Gaussion distribution calculated from LSS theory.

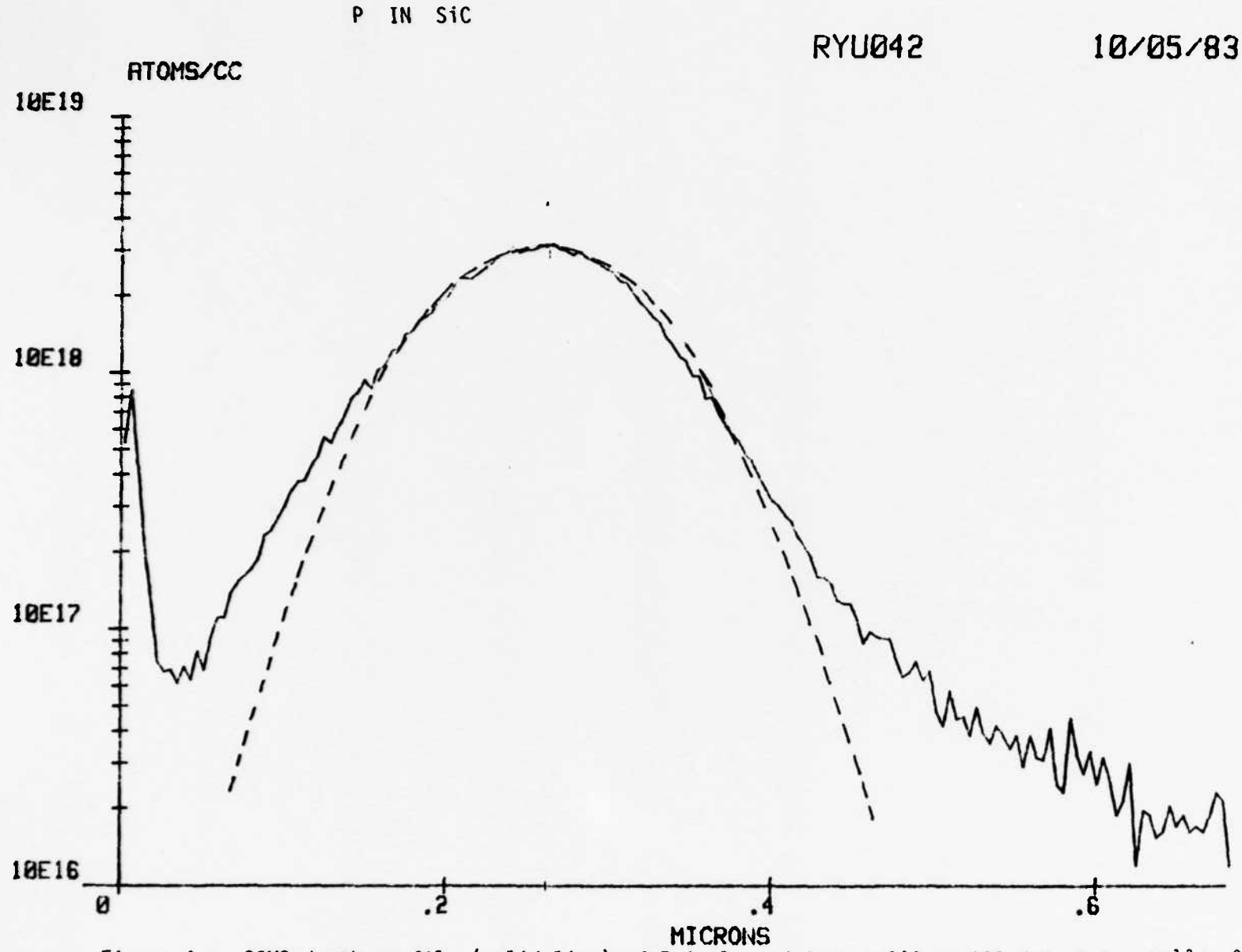

Figure 4. SIMS depth profile (solid line) of P implanted into β-SiC at 300 KeV, $7.5 \times 10^{13}/cm^2$ and room temperature. Broken line is the Gaussion distribution calculated from LSS theory.

TABLE I. Ion implantation conditions for the profiles of Figs. 2-4 produced in β-SiC thin films.

Ion	Total Energy, Kev	Source	Dose cm^{-2}	Peak Conc, cm^{-3}	Sample Orientation	Degree of Off-set	Temperature
$^{11}B^{+}$	200	BF_3	$7.6x10^{13}$	$4.7x10^{18}$	(100)	7°	ambient
$^{14}N^{+}$	200	N_2	$1.5x10^{15}$	$1.2x10^{20}$	(100)	7°	ambient
$^{31}P^{+}$	300	PH_3	$7.5x10^{13}$	$3.2x10^{18}$	(100)	7°	ambient

TABLE II. Equipment parameters employed and results derived from ion microprobe depth profiling of representative samples of implanted β-SiC.

Exp.Cond./ Dopant	Primary Ion	Primary Ion Current (namp)	Accel. Volt. (kV)	Raster Width (μm)	Transfer Optics Slit (μm)	Field Aparture No.	Control Aparture No.	Sputtering Rate (Å/sec)	Min.Deter. Range (Atoms/cm^3)	Peale Concentration Position (μm) LSS	Dektak
B	Oxygen	1310	15.1	100	150	2	3	20	1.5×10^{18}	0.47	0.38
N	Oxygen	992	15.1	150	150	2	3	8.7	1.3×10^{16}	0.35	0.31
P	Cesium	514	12.8	250	150	2	2	4.7	2×10^{16}	0.26	0.24

determine the actual peak position or the position of any other concentration.

A perusal of Figs. 2-4 shows that the minimum detectable limits for B and P are approximately 10^{16} atoms/cc (it is actually $\approx 10^{15}$ for B if special care is taken to tune the instrument); however, for N it is only $\approx 5 \times 10^{17}$. This last detection limit somewhat complicates electronics research in SiC; since N is (1) often accused of being a frequent and uncontrolled impurity in SiC (this writer is becomong skeptical of the validity of this claim, in many cases because of the difficulty in decomposing N_2 even at high temperatures), and (2) difficult to detect even semiquantitatively at levels less than 10^{18} by any other analytical method than high resolution SIMS. Charge carrier concentrations can be measured electronically but this usually does not equal the total dopant concentration as noted above. The problem for N in SIMS analysis is that it has one of the highest ionization potentials and lowest electron affinities thus making the formation of secondary ions difficult. It is also difficult to separate from Si^{2+} and CH_2 which have virtually the same mass. However, at NCSU and within this program, the investigators have developed and employed the energy offset method which allows the detection of N at the lowest possible levels. Figure 5 illustrates our developed capability to mass separate N from Si^{2+} and CH_2.

Finally, the ion microprobe is also equipped with a Cs^+ primary ion source, necessary to analyze $^{31}P^+$. High resolution mass filtering is also necessary for this species in order to separate it from $^{31}SiH^+$.

Although it is not shown in the figures of the implanted profiles included in this report, the numerical values of the ion yield of Si were also obtained with the ion microporbe at the same time the ion yields of the various dopants were measured as a function of depth. Thus any slight changes in primary beam current or of the optics or readout of the instrument thus affected both species. From this information, the ratio of the secondary ion count of each dopant to the total Si count could be calculated for a series of points along the depth profile. Since the depth profile varies in dopant concentration from the minimum detectable limit for that species to the maximum in each profile, and these concentrations are known from the ion implant standards, as

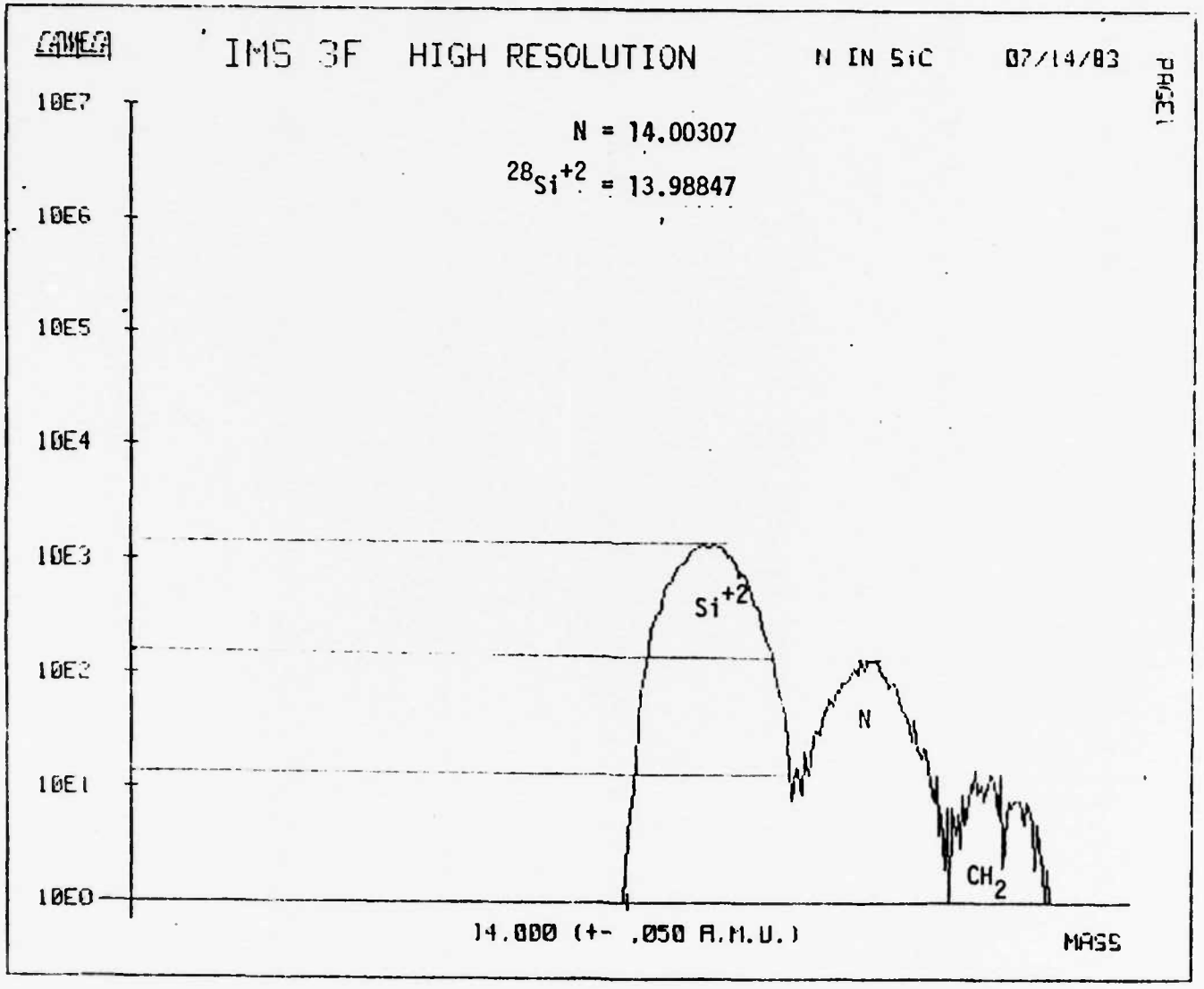

Figure 5. Illustration of the use of the CAMECA ims-3f high resolution mass separation capability for $^{28}Si^{2+}$, ^{14}N and CH_2. The mass difference of $^{28}Si^{2+}$ and ^{14}N is only 0.015 amu.

noted above, one may plot the aforementioned ratio as a function of dopant concentration as shown in Figures 6-8 for B, N and P. The resulting graphs are very linear; their most important use will be in the determination of the amount of dopant introduced during in-situ growth. Since the in-situ doped samples will be evaluated with the ion microprobe for the variation in dopant level as a function of flow rate of the dopant gas or H_2 (in the case of Al) or the temperature of the Al source, a dopant count/Si count ratio can easily be attained and, from Figures 6-8, the exact concentration of dopant in the as-grown samples determined. Most importantly, this chemical concentration can now be compared with the electrically measured charge carrier concentration in the in-situ doped samples and in the implanted samples as a function implant dose and annealing schedule.

3. Annealing of the Ion Implanted β-SiC

Ion implantation causes structural damage to the solvent crystal of a magnitude which is a function of the implant dose. As such a large proportion of the dopant atoms are usually not situated on electronically active sites, the samples must be annealed to properly locate both solvent and solute atoms to their equilibrium lattice sites and to remove lattice and dislocation damage remaining after regrowth to mitigate charge carrier traps.

To date, we have employed commercially produced rapid thermal annealing (RTA) equipment which employs a quartz lamp as well as thermally annealing on an SiC-coated strip heater in a bell jar confinement. The RTA, though very effective for Si implants, only slightly (0.08 μm) altered the implant profile and produced little charge insofar as enhanced electrical activity is concerned. The maximum temperature and time of this group of anneals was 1473K and 300 s. Many different heating schedules were investigated, but the very strong bonding in β-SiC causes the rate of atomic vibrations and resultant atomic transport to lattice sites to be very much reduced relative to Si at 1473K.

Because of the problems encountered with RTA, special SiC-coated graphite strip heaters of the same materials used to produce the CVD susceptors have been developed for annealing at higher temperatures.

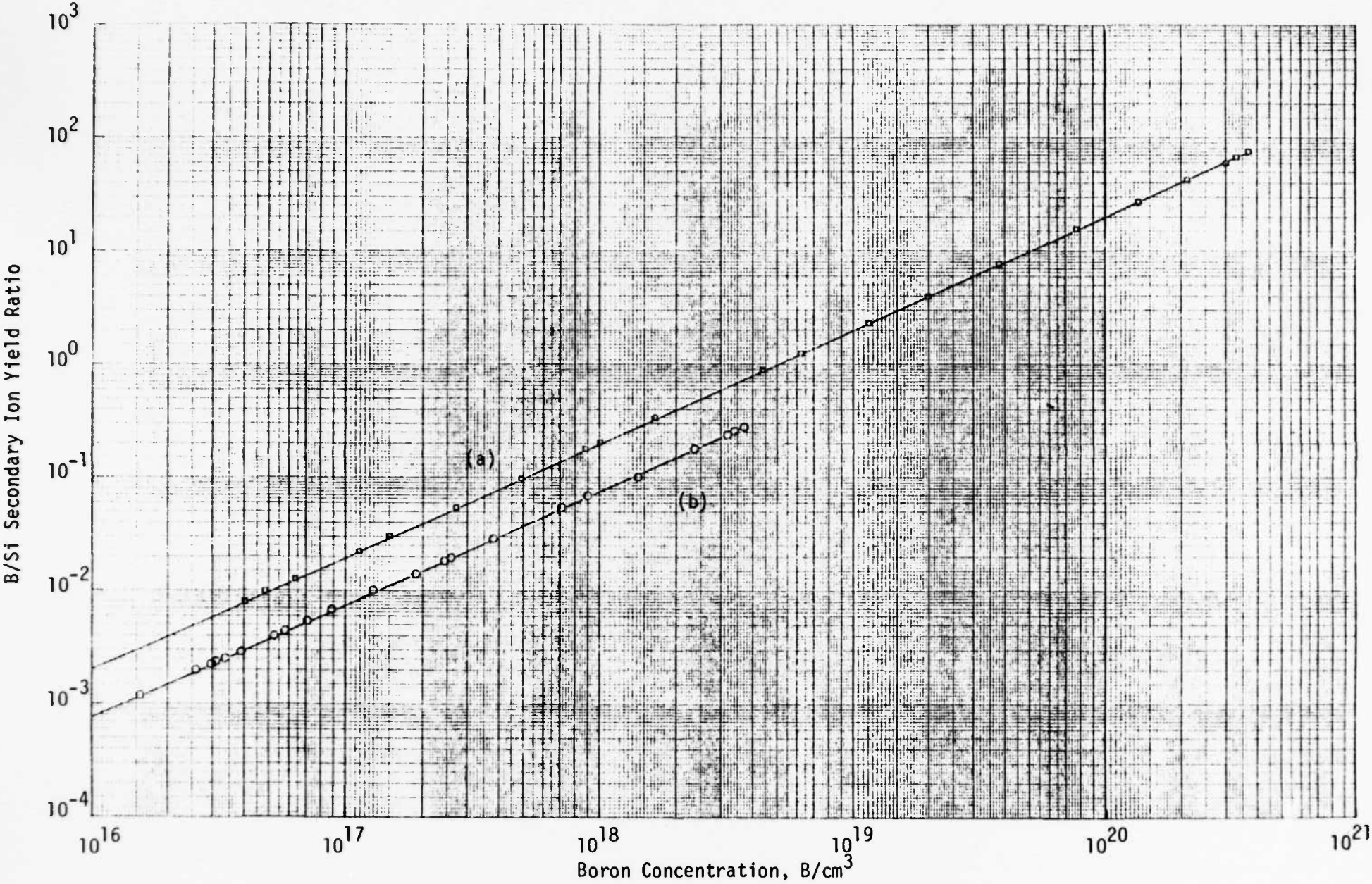

Figure 6. The B/Si secondary ion yield count ratio obtained from low to maximum concentrations in SIMS depth profiles of B ion implants made at 200 KeV and dose levels of 7.58×10^{15} B/cm^2 (curve a) and 3.72×10^{13} B/cm^2 (curve b).

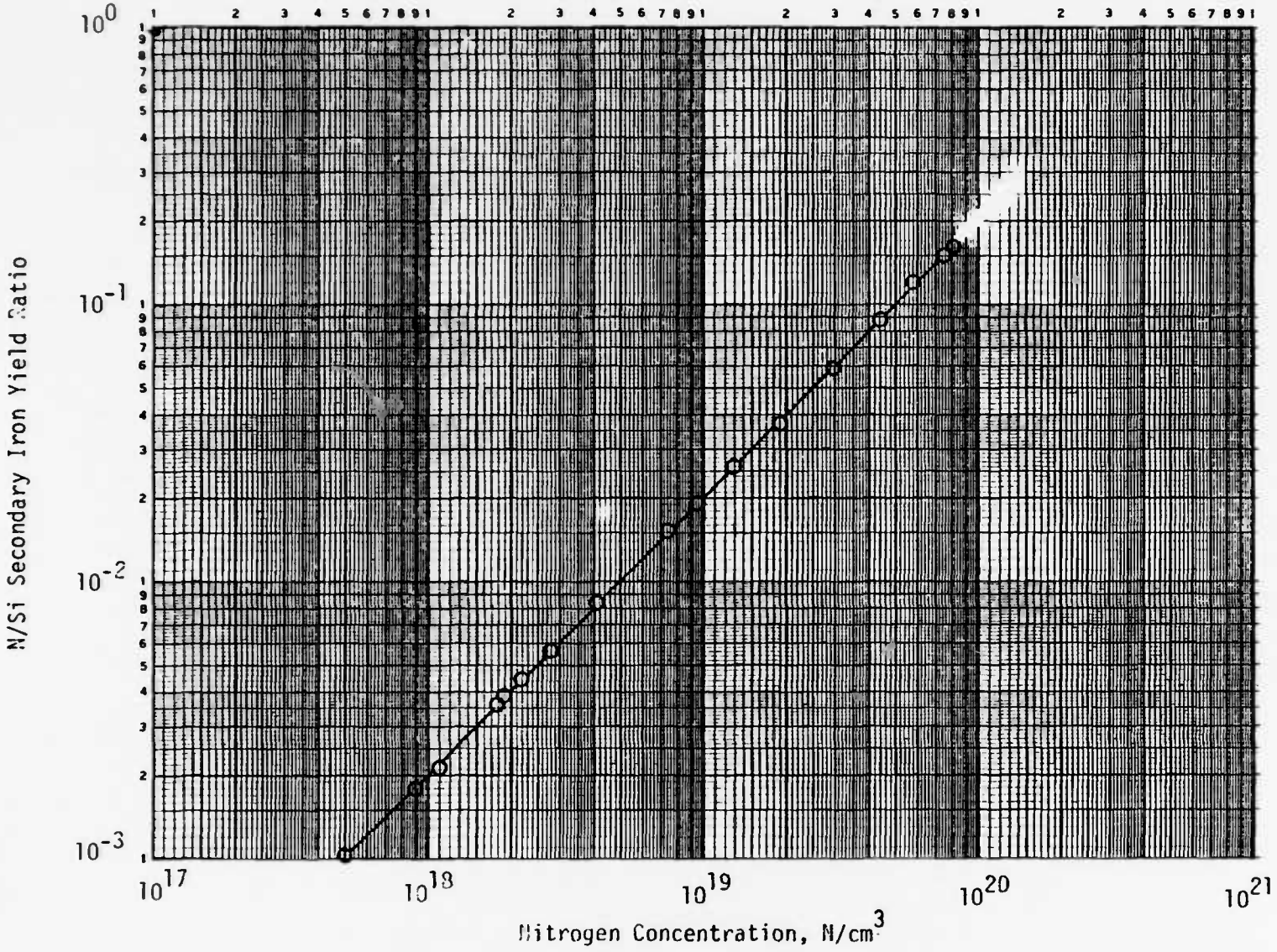

Figure 7. N/Si secondary ion yield count ratio obtained from low to maximum concentrations in SIMS depth profiles of a N ion implants made at 200 KeV and 1.5 x 10^{15}/cm^{2}.

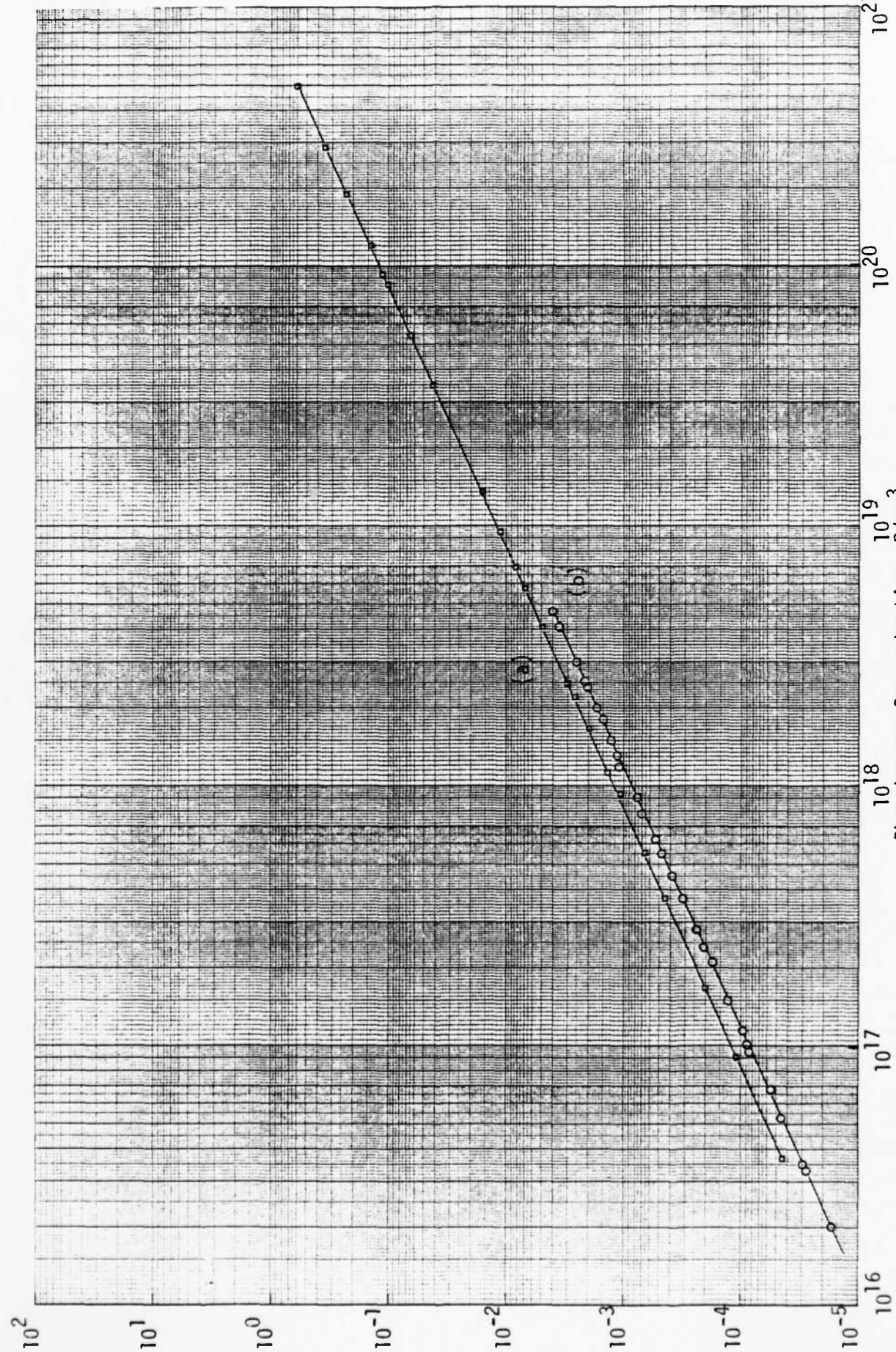

Figure 8. P/Si secondary ion yield count ratio obtained from low to maximum concentrations in SIMS depth profiles of P ion implants made at 300 KeV and 7.95 x 10^{15} P/cm^2 (curve a) and 7.5 x 10^{13} P/cm^2 (curve b).

A thermal evaporator has been retrofitted to handle these heaters and to provide sufficient power for heating to approximately 2273K. Preliminary results to date show that annealing near to the melting point of Si only slightly affects the incorporation of the dopants on the lattice sites. As such, we are now developing techniques for removing the β-SiC from the Si in order that much higher temperature anneals can be conducted. It is anticipated that Rutherford Backscattering in the Channeling Mode (available at UNC, Chapel Hill in a "stand alone" instrument and at NCSU as an "add-on" instrument to the 400 KeV ion implanter) will have to be used in conjunction with electrical measurements and ion microprobe analysis in order to determine structural changes as well as chemical and electronic during annealing. This will probably be the most difficult and time consuming task yet encountered in the program.

Finally, we have also produced triple Si implants in the same sample, the maximum depth of which exceeds the implant depth of the dopant (also in same sample). In this way the residual damage (dislocation loops, etc.) which normally occurs at the implanted layer/unimplanted material interface after annealing will be produced where the end of the Si implant occurs and not at the end of the dopant profile where it can getter the dopant.

III. Electrical Properties

In order to conduct electrical measurements concerned with the I-V characteristics of the as-grown intrinsic or doped samples, the implanted and annealed samples and future devices, proper ohmic contact materials must be available for both n-type and p-type materials. Based on prior art and our own research, we have developed such materials which consist of a 3% Ta/97% Au alloy for n-type SiC and a 2.3% Ta/7.3% Al/90.4% Au alloy for p-type SiC. It was also found that an 11% Si/89% Al alloy was ohmic on p-type SiC; however, its melting point is ≈823K.

We have employed Hg-probe techniques to conduct C-V measurements in order to obtain the charge carrier concentrations in the many as-grown sanples. To date, the calculated results indicate a range of carrier concentrations from 4×10^{15} to $9.3\times10^{17}/cm^3$. The average is approximately $8\times10^{16}/cm^3$.

We have also planned and are now having fabricated a high and low temperature Hall measuring unit. This will be discussed in the next report. We have also developed a technique for making the standard clover leaf shape on the β-SiC for van der Pauw measurements. In this process, a brass mask is paced over the β-SiC film and the uncovered portion of the film abraded with 30 micron B_4C grit. We will be using samples made in this way to obtain the ionization energies of the dopants and carrier mobility as a function of temperature. This will be coupled with additional research on laser photoluminesce in the Physics Department at NCSU with Professor Paesler.

IV. Chemical and Physical Characterization of the Chemically Converted Layer on Silicon

A. Introduction

As noted in the introduction, we have found empirically that micro-crack free β-SiC can be grown on single crystal (100) Si substrates if the Si is initially reacted with flowing C_2H_4 in H_2 for approximately 150 s. This step allows a gradient in the thermal expansion coefficient and the lattice parameter to form such that β-SiC thin films of virtually any thickness can be subsequently produced.

The present study, though unique in its objectives and its collective modes of characterization, has been preceded by several reports of the fabrication of similar SiC thin films on Si single crystals via several different routes. Some of these studies have concentrated wholly or in part on the mechanisms of SiC formation but have reached different conclusions concerning this point. These prior studies can be separated into two groups according to the growth techniques employed: (1) reaction of the Si substrate with a hydrocarbon gas contained in a flowing gas mixture under conditions of viscous flow*[1-5], and (2) reaction of the Si substrate surface in high (HV) or ultrahigh (UHV) vacuum chambers at a hydrocarbon partial pressure corresponding to molecular (free)

---

* The flow regime can be determined by Knudsen's number, $K_n = \lambda/d$, where λ = the mean free path of the gas atoms in the system and d = the minimum physical dimensions of the system. A viscous flow condition occurs when $K_n << 1$ in a system [6]. The character of the fast flow in this regime is determined by gas-gas collisions.

flow.* Various hydrocarbons such as C_2H_2 [8,9,11-13], C_2H_4 [8-10], C_3H_8 [5], and CH_4 [1-4], or even the graphite susceptor (regular and pyrolytic) [15], have been used as the C source to convert a Si substrate surface into β-SiC.

Saturated hydrocarbons (e.g., CH_4 and C_3H_8) have been used in the first technique, which requires temperatures in excess of 1373K at a total pressure near 0.1 MPa for viscous flow; while unsaturated hydrocarbons (e.g., C_2H_4 and C_2H_2) have been used in the second technique, in which temperatures as low as 1073K may be employed under HV or UHV conditions. The substantially lower growth temperature for the vacuum growth environment than for the near-atmospheric pressure environment is because (1) the unsaturated hydrocarbon decomposes relatively easily and at lower temperatures, and (2) the condition of vacuum enhances the decomposition of the hydrocarbon as well as the desorption of H_2 produced on the growing surface in the absence of an H_2 carrier gas. A review of several selected studies which illustrate the range of results obtained is presented below. Reaction under viscous flow conditions will be considered initially.

Tombs et al. [15] were one of the first investigators to grow highly adherent epitaxial films of β-SiC on single crystal Si substrates by the reaction of the latter with C derived from spectrographic grade of a pyrolytic graphite susceptor heated to ≈1523K in a 0.1 MPa stagnant atmosphere of purified Ar. Selected area and reflection electron diffraction revealed that the films were polycrystalline at or near the Si/SiC interface, but changed to monocrystalline near the final surface. Thickness values of 2.5×10^{-6} and 10×10^{-6} m were obtained for growth times of 300 and 1800 s, respectively. The mechanisms of formation and growth were attributed to the initial substitution of C for Si in the substrates followed by diffusion of C through the growing β-SiC layer. However, the reported [16] solubility of C in Si just above the melting point of the latter (1681K) is only 5×10^{-3} mol% (5×10^{17} C atoms/cm^3 Si);

---

* The condition of (free) molecular flow occurs when $K_n \geq 1$ in a system [6]. The flow properties in this regime are determined by gas-wall collisions. (Note: The transition from viscous flow to molecular flow and vice versa is not sharp but gradual. Therefore, when $0.01 < K_n < 1$ [7], the flow condition is termed "transition flow."

thus, at 1523K only a very small amount of C would be substituted for Si.

Spitzer et al. [1] were one of the first to react a single crystal Si surface with a C-containing gas, namely methane (CH_4) carried in argon at 1573K. Although the study concentrated on infrared transmission and reflectance measurements, little information was reported concerning the film, except that it was polycrystalline β-SiC having a thickness of approximately 0.11×10^{-6} m.

Studies by Nakashima et al. [2] concerned with the reactions of Si single crystals with CH_4 in the temperature range of 1483-1573K showed that this reaction obeys the parabolic rate low with an activation energy of $\tilde{\sim}4$ eV/atom. Furthermore, the growth rate is proportional to the partial pressure of CH_4. Based on this knowledge alone, these authors surmised that the rate determining process may be attributed to the diffusion of C through the SiC film. As in the results noted by Tombs et al. [15] and Spitzer et al. [1], the as-grown film was observed to be epitaxial and polycrystalline at the Si/SiC interface but monocrystalline on the surface.

Graul and Wagner [3] have also investigated the mechanism of polycrystalline SiC layer growth on monocrystalline Si by employing radioactive ^{14}C-containing CH_4 carried in H_2. These authors observed that the growth rate of SiC was a function of the CH_4 concentration in the H_2 carrier gas up to 2 vol% at 1523K. Above this concentration, these authors concluded from an unusual analysis of the diffusion profiles that the growth occurs by grain boundary diffusion of Si through the growing layer such that the Si-SiC conversion occurs at the gas/layer interface. This conclusion is in direct contrast to those of Tombs et al. and Nakashima et al. noted above. The one ^{14}C concentration profile reported by Graul and Wagner is similar to the C profiles obtained by ion microprobe analysis of the SiC layers grown in the present research and discussed below.

Epitaxial films grown in both HV and UHV systems exhibit characteristic "pit" and "hillock" type defects [8-13] in addition to the usual crystallographic defects (stacking faults, twins, etc.) commonly found in thin epitaxial films.

Haq and Kahn [12] measured an unusually high electrical conductivity and the complete absence of a surface barrier in (111)β-SiC films grown on (111)Si single crystal wafers using C_2H_2 under the conditions of 1223K and 10^{-6} torr. Multiple-beam-interference fringe patterns obtained from the surface of a 10^{-6} m thick film indicated local elevation differences of ≈300 nm on the surface. Scanning electron microscopy revealed the defects to be predominantly depressions which frequently contained "hills" in the interior. From these and additional electrical measurements on layers which had been removed from the Si, it was concluded that these surface defects acted as recombination centers, thereby causing the disappearance of the surface barriers. Slight nonstoichiometry in the SiC itself or, more likely, the existence of a layer containing two phases, e.g., C and SiC and/or a significant degree of crystallographic defects inside the layer may also play major roles in the high conductivity.

Somewhat similar β-SiC growth and defect patterns have been observed by Brown and Watts [10] using C_2H_4 at 10^{-6} torr in the temperature range of 1173-1523K. Epitaxial growth of discrete β-SiC particles was observed on (100) (111) and (311) monocrystalline Si substrates. Etch pits were observed on substrates of all orientations irrespective of the presence of ethylene unless the substrates had been previously thermally cleaned by heating to ≈1500K for 600 s in an ultra-high vacuum ($5x10^{-10}$ torr). The SiC particles formed inside and outside the pit areas when present on the Si surface.

A related but more extensive study of the conversion of Si to epitaxial SiC has been conducted by Mogab and Leamy [17]. The experimental conditions employed in this research included the use of C_2H_2 in both HV and UHV chambers in the pressure and temperature ranges of $10^{-7} \leq P_{C_2H_2} \leq 5x10^{-4}$ torr and $1073 \leq T \leq 1373$K, respectively. Several surface preparation steps and HV and UHV preannealing steps were investigated for the Si wafer. These authors concluded that the occurrence of defects in the Si is intrinsic to the mechanism of film growth. This mechanism was presumed by these investigators to be (1) the diffusion of Si through porous defects incorporated in the growing film as a result of the concurrent formation of similar defects on the Si surface and (2) the

subsequent reaction of this Si with the C in the C_2H_4. The resultant SiC assumes a porous polycrystalline morphology around these shallow (<200 nm) pits in the Si substrate which are assumed to be the sources of Si for the reaction. The number and real density of the defects in the SiC layer are proportional to the partial pressure of C_2H_2 and the SiC film thickness. At $P_{C_2H_2} > 10^{-5}$ torr, these defects in SiC are sealed at an early stage in the growth and further reaction is virtually arrested as a result of decreased diffusion rates. The type of vacuum system employed was not a factor in the growth process.

V. Experimental Procedure

A. Thin Film Growth

Semiconductor quality, p-type (ρ = 10-20 kohm-cm) single crystal Si wafers having a diameter and a thickness of 0.01 m and $5x10^{-4}$ m, respectively, and sliced precisely along the (100) crystallographic faces were used in this study as substrates on which to incrementally grow the converted layer and the β-SiC thin films. All wafers were subjected to a chemical-mechanical polishing using a slurry of cupric nitrate ($Cu(NO_3)_2$ $3H_2O$) and ammonium fluoride (NH_4F) in H_2O without any abrasive medium. After polishing, the concentration of residual Cu was readily reduced with dilute HNO_3 to <10 ppb. No further surface preparation was employed.

The wafers were placed on a SiC-coated graphite susceptor (which had been precleaned in flowing Cl_2 at 2373K) and located in an rf-heated CVD chamber. The chamber was pumped to 10^{-6} torr and backfilled to 760 torr with the H_2 carrier gas which was continuously purified via Ag/Pd diffusion cell. Research grade C_2H_4 (99.99% pure) was subsequently introduced and equilibrium flow rates of this gas and that of H_2 were established at 1.0 sccm and 3000 sccm, respectively.

The susceptor/wafer system was heated at approximately 500K/min by immediately increasing the power output of the rf motor generator to a level which had been empirically predetermined to produce the optimum converted layer for subsequent growth of the highest quality β-SiC thin films.

Although it had been previously determined that heating the wafers for a period of 150 s after the application of rf power to the susceptor produced the optimum converted layer for subsequent thin film growth,

for this study the time of heating was varied from 120 s to 210 s in 30 s intervals, in an attempt to understand what changes occurred throughout the layers as a result of the varying times and temperatures of growth (see next paragraph) and to characterize the final surface of each layer.

Because of its mass, the temperature of the susceptor/wafer system continued to increase throughout the 120 s and 150 s runs. The final maximum temperatures for these times were 1553 and 1603K, respectively. For the 180 s and 210 s runs, the maximum possible temperature of 1633K was achieved at some point in the experiment. An optical pyrometer was used to measure the temperature of the SiC-coated graphite; since continuous corrections for emissivity and changes in this emissivity as a result of continous deposition were unnecessary, in contrast to the situation for the Si wafers.

Following the desired conversion time, the flow of C_2H_4 was interrupted, the system heated for an additional 30 s in flowing H_2 and the power reduced rapidly to zero. The system was subsequently purged with research grade Ar and the wafers removed for analysis.

B. Characterization

Changes in composition of the converted layers as a function of depth were determined using secondary ion mass spectometry (SIMS). For these analyses, the CAMECA ims-3f ion microprobe and its mass-filtered Cs primary ion source were utilized. The configuration of the instrument for this study included a primary ion current of approximately 100 nanoamps, depending on the run, a primary voltage potential of 17.3 kilovolts, a beam size of 25×10^{-6} m, a rastered field of 250×10^{-6} m and a signal acceptance field of 60×10^{-6} m. The layers as well as a 5×10^{-6} m thick single crystal β-SiC reference film were analyzed for the isotopes of ^{12}C, ^{30}Si, ^{16}O and the presence of the impurity ^{27}Al to a depth sufficient to allow the ^{12}C signal to be reduced to background levels. The rate of profiling was estimated to be approximately 0.95 Å/s based on angstrometer measurements of the depths of several pits placed into the β-SiC thin films for various time periods using the same primary ion current and size of rastered field. The location of the profiles of the various Si/C ratios reported in the Results section were determined using the ratio of

the signal counts of ^{30}Si and ^{14}C in the reference standard which is that for pure SiC. This latter ratio of a multiple thereof was located in the signal outputs of the profiles of the converted layers and the depths of these points calculated knowing the rate of profiling and the duration of each analysis.

The X-ray photo electron spectroscopy (XPS) measurements provided information concerning the composition, types of chemical species present and the binding energies of the species at or near the final surfaces of the converted layers, the standard reference film and the (0001) face of an α-SiC single crystal standard. For this research, a Physical Electronics Model 548 electron spectrometer having a MgK_α($h\nu$ = 1253.6 eV) X-ray source was employed. Each of the samples was mounted on an Al sample holder by means of an Mo mask and transferred via load lock into the primary chamber having a vacuum of 10^{-9} torr. Samples were carefully positioned so as to be centered in front of the electron analyzer and to minimize holder interference. An initial survey scan (0-1000 eV, 100 eV pass energy) was acquired to determine the presence of contaminants. This was followed by higher resolution "window" scans (25 eV in width, 25 eV pass energy) to determine more accurately and quantitatively the binding energies and peak areas. The samples were then ion etched with an Ar^+ ion beam (2 keV, 20 m A beam current) for five or ten minutes. Survey and window spectron were then reacquired. All data for the individual elements was corrected using sensitivity factors taken from the Physical Electronics Handbook.

IV. Results and Discussion

A. SIMS Depth Profiles

The depth profiles for $^{30}Si^+$, $^{16}O^+$, $^{12}C^+$ and $^{27}Al^+$ in the converted layers and for a portion of the Si substrate are shown in the figures 9-12 for each of the growth times. Figure 13 shows the $^{30}Si^+$, $^{16}O^+$ and $^{12}C^+$ for the standard β-SiC thin film. The ordinate and abscissa of each graph are the number of counts and the data channel number, respectively. The characteristics of three of the important points in these profiles are given in Table III. The depth of a particular point may be calculated knowing the sputtering rate (given in the figure captions) and the total time employed to obtain the profile (given in the right hand

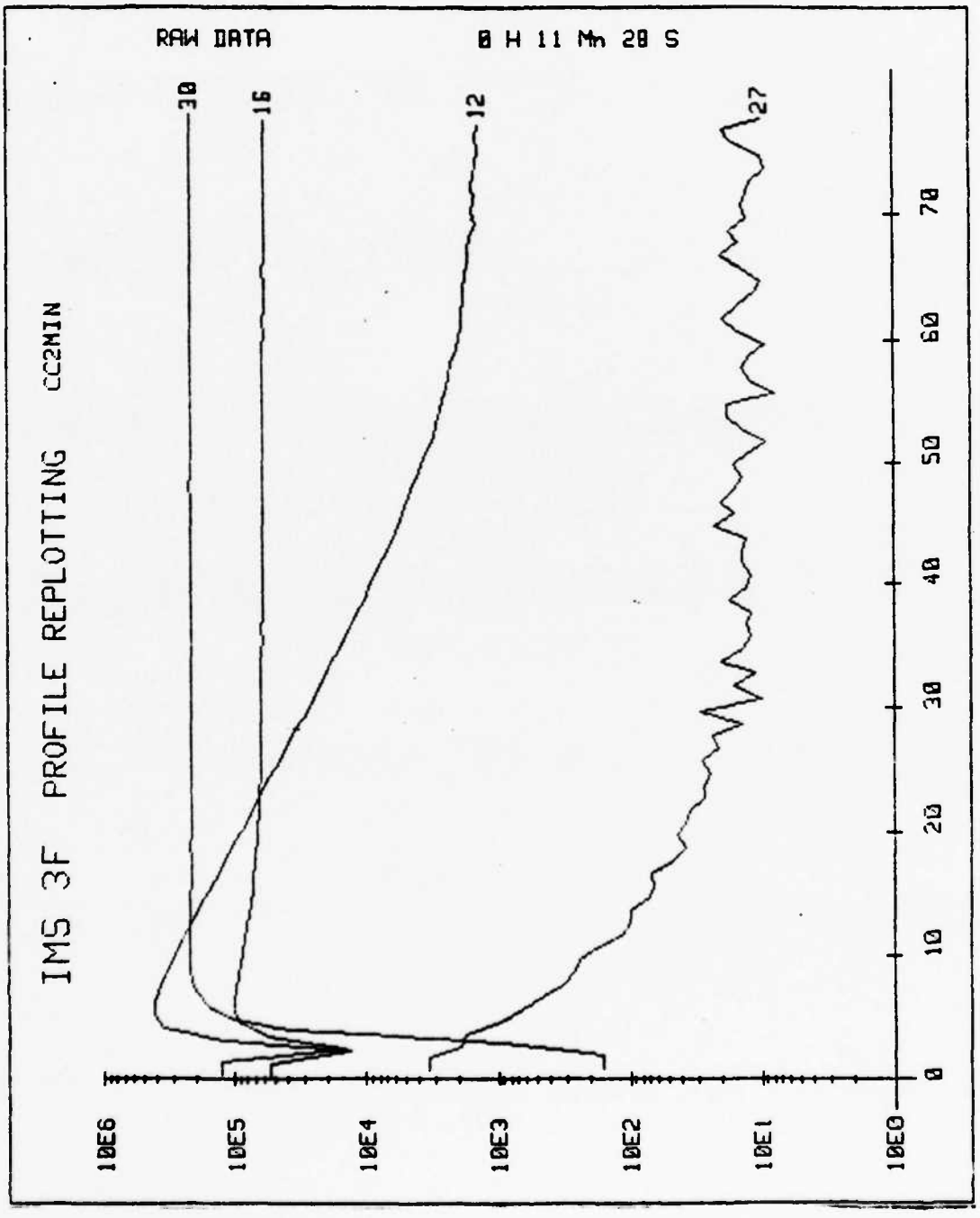

Figure 9. SIMS depth profiles for Si, O, C and Al in a converted layer having a growth period of 120s. The profiling rate and primary ion current were 0.90 Å/S and 103nA, respectively.

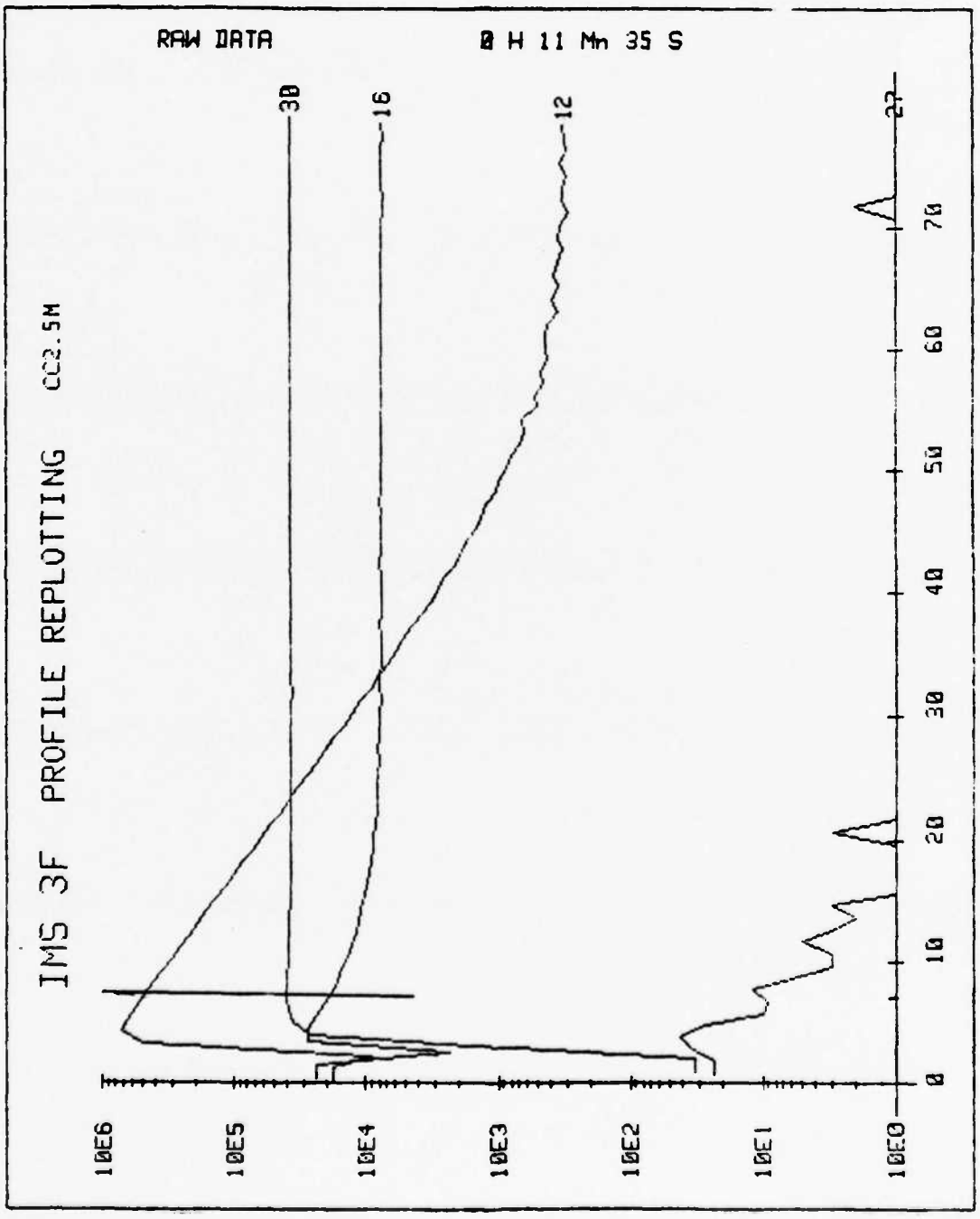

Figure 10. SIMS depth profiles of Si, O, C and Al in a converted layer having a growth period of 150s. The profiling rate and primary ion current were 1.03Å/S and 118nA, respectively. Vertical line represents position where Si/C = 1:1.

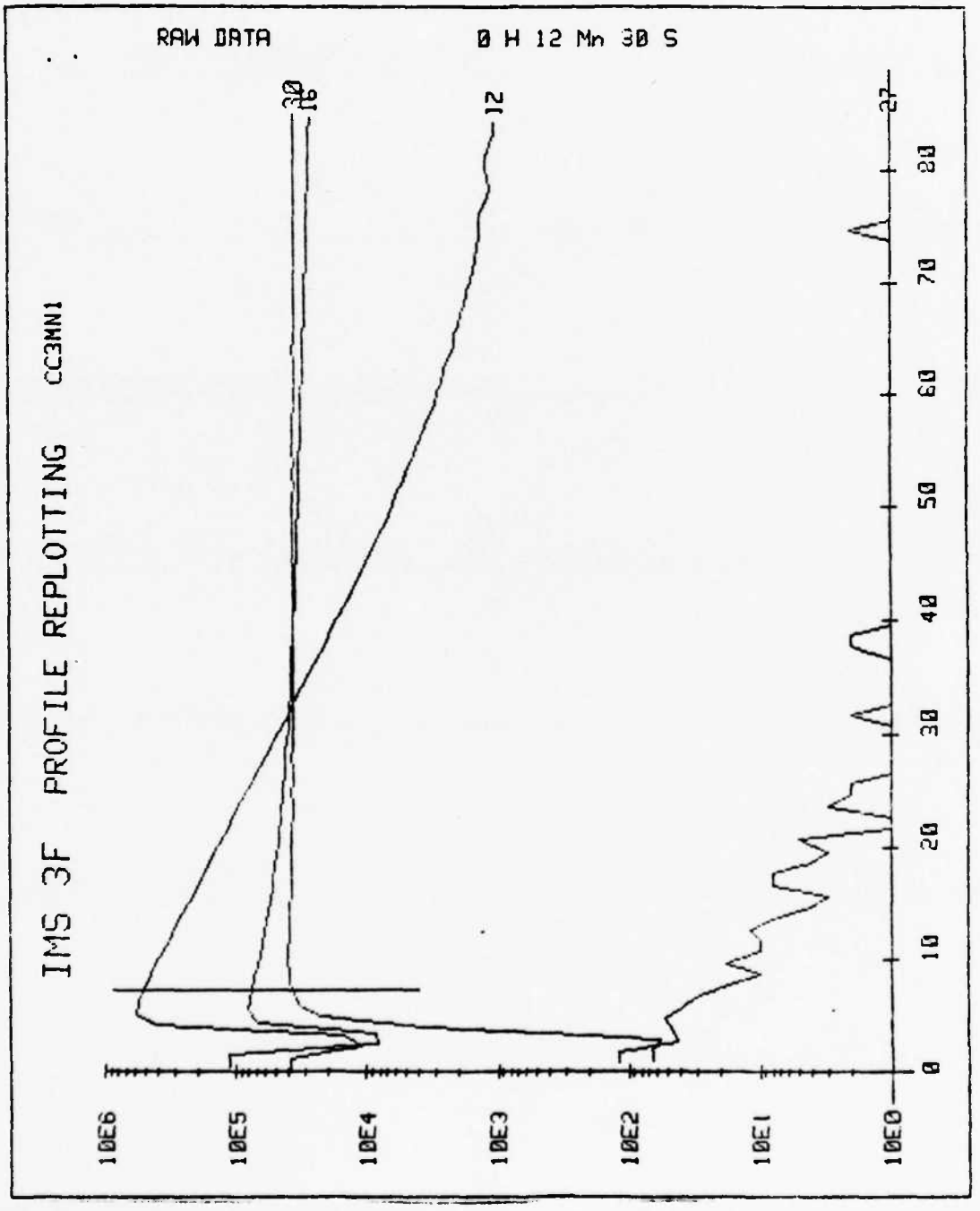

Figure 11. SIMS depth profiles of Si, O, C and Al in a converted layer having a growth period of 180s. The profiling rate and primary ion current were 0.85 Å/S and 97nA, respectively. Vertical line represents position where Si/C = 1:1.

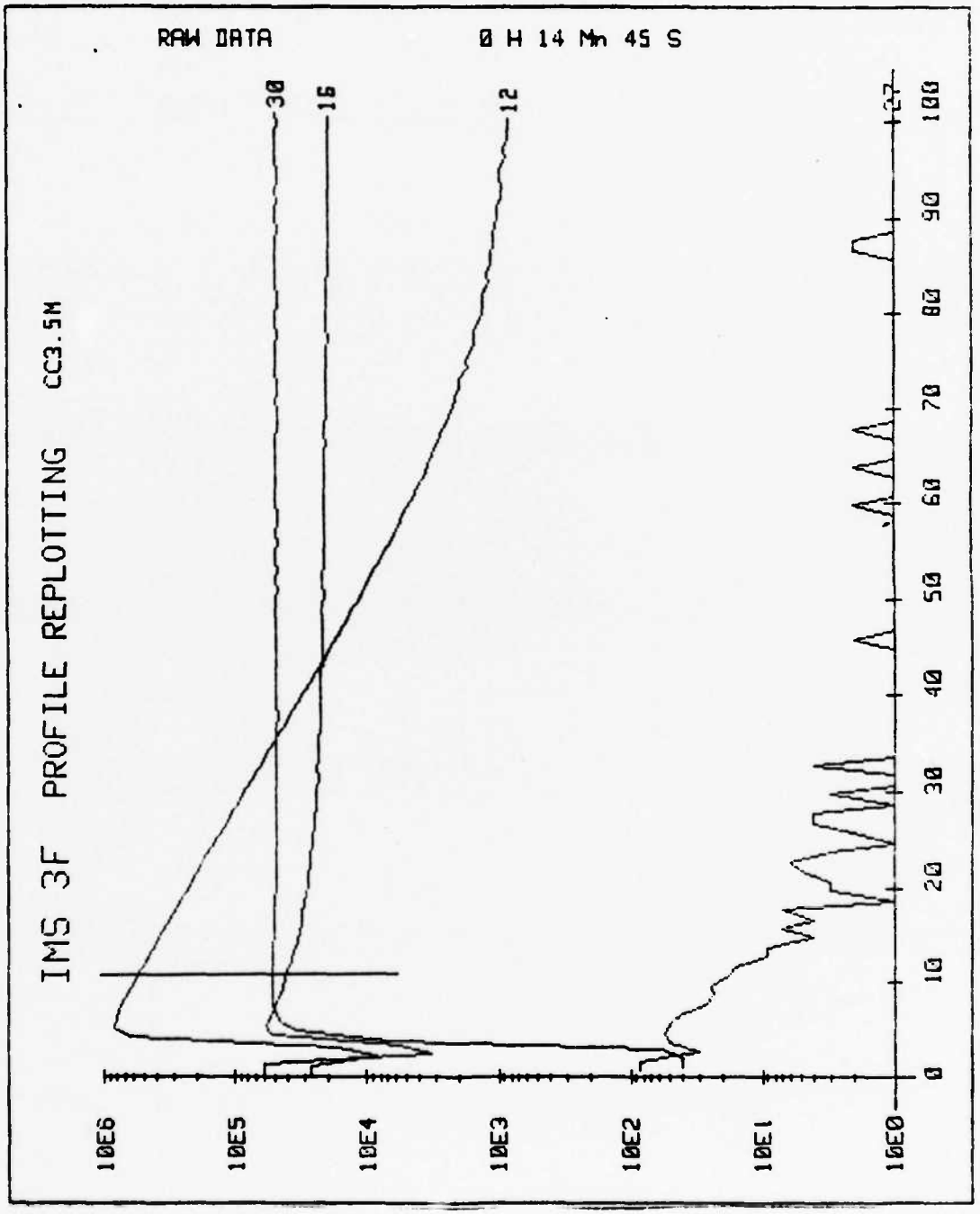

Figure 12. SIMS depth profiles of Si, O, C and Al in a converted layer having a growth period of 210s. Sputtering rate and primary ion current were 1.00 Å/s and 114nA, respectively. Vertical line represents position where Si/C = 1:1.

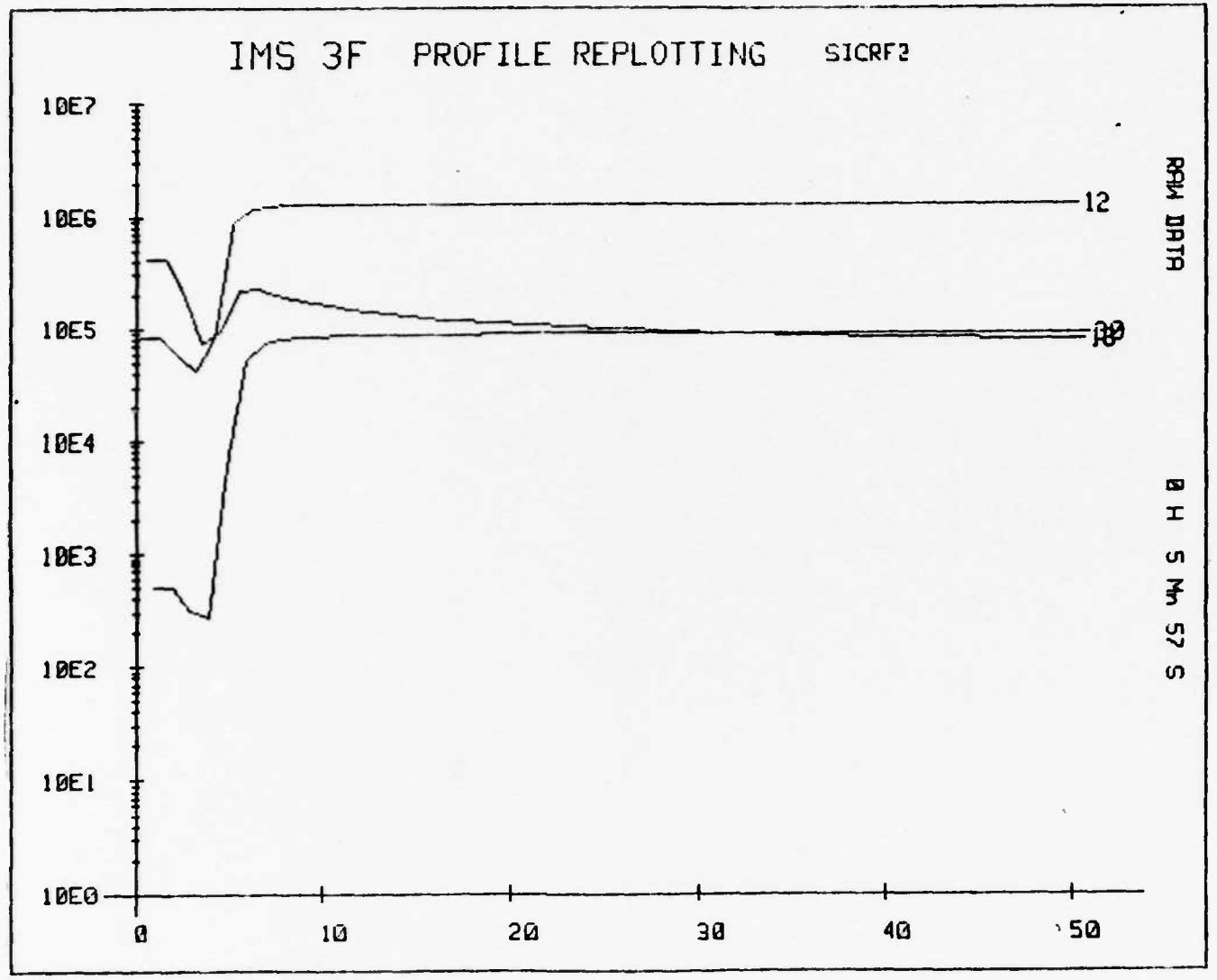

Figure 13. SIMS depth profiles of Si, O, and C in the β-SiC thin film (≈5 x 10^{-6}m thick) standard. The rate of profiling and primary ion current were 0.902 Å/S and 103nA, respectively.

TABLE III. Characteristics of three important points in the concentration profiles of Si and C in Figures 9-12, including the depth and the Si/C atom ratio in absolute terms as well as normalized relative to the β-SiC thin film standard.

Sample # (time of growth in seconds)	Point of Max. Carbon Concentration			Point Where Si/C = 0.071			Point Where Si/C = 30	
	distance A	Si/C	normalized Si/C	distance A	Si/C	normalized Si/C	distance A	Si/C
120	48.4	0.46	6.48	N.E.	0.071	1.0	376.2	30
150	37.2	0.045	0.63	60.6	0.071	1.0	432.5	30
180	42.6	0.060	0.84	52.8	0.071	1.0	606.8	30
210	52.0	0.052	0.73	91.8	0.071	1.0	679.4	30

margin of each figure). The very top surfaces of the samples contain various hydrocarbon and loosely-bonded oxygen-containing species such as OH^- which contribute to the high levels of these species at the very beginning of the profiles. Following their removal, the count rates for these profiles decrease immediately and are succeeded by a rapid increase in the count rates for all the species except $^{27}Al^+$. This increase in count rate probably represents the removal of an SiO_x layer to a depth wherein each of the C profiles has its maximum value. This is also the position of the final growth surface of the converted layer. This distance is given in Table III for each of the four samples.

The $^{27}Al^+$ profiles were determined in order to ascertain if any Al existed at the surface as an impurity as was observed in a few samples produced much earlier in the program. Except for the 120s sample, the concentration of this element was very low even at the surface and decreased rapidly to background after a few angstroms of sputtering. Thus it is not considered a problem at this time.

The $^{16}O^+$ was determined in an attempt to ascertain if it was possible to detect this element in the films above the background level. Although a Cs primary beam was used for this study both O^+ and O^- beams are more commonly employed. Thus, everything in the primary column has a thin oxide coating. Briefly, detection of O in the films above the background level was not possible. However, this important question will again be pursued via XPS studies.

The most interesting portion of each of the profiles is the changing relationship between Si and C and a function of depth and time of chemical conversion. The determination of the ratio of the Si counts to the C counts for a pure β-SiC thin film standards allowed the calculation of the actual Si/C ratio at the point of maximum concentration and the determination of the point in each profile where the Si/C atom ratio is equal to 1.0 (given as a vertical line in each of the profiles). A Si/C ratio of 30 (see Table III) was used as a somewhat arbitrary point at which the C concentration was assumed to be reduced below background levels.

In the 150, 180 and 210s profiles, the initial surface (assumed to be at the point of maximum C concentration) has a Si/C <1 compared

to the 1:1 ratio for the β-SiC thin film standard. This indicates that the surface is C-rich. For the 120s sample, the surface is apparently very Si-rich indicating very little C-Si reaction and/or some sampling of the underlying Si layer via pinholes and unreacted areas.

The Si concentration increases rapidly to a very steady level which is essentially maintained throughout the entire thickness of each layer. By contrast, the C concentration falls rapidly in each case reaching a point where the Si/C = 1.0 within 90 Å of the surface. The concentration at which the C is at-or-below instrument background is within 370-700 Å, depending on the reaction time.

Since there is very little solubility of C or Si in SiC or C in Si at the temperatures of growth, it seems reasonable from these results (and those derived from XPS - see next section) that at and near the surface of the 150, 180 and 210s samples one has a dominant matrix of β-SiC containing some free C. The amount of β-SiC increases slightly over a few Å but thereafter decreases in amount such that the microstructure changes to contain diminishing amount of β-SiC and an increasing amount of Si. It is also very possible that the surface of each of these three samples is pure β-SiC. However, at the onset of sputtering, the Si is removed preferentially until equilibrium is established between the sputter rates of both Si and C. Plasma sputtering studies would indicate that although there is preferential sputtering initially, equilibrium is established after a few angstroms and the initial (or actual) composition is sputtered thereafter.

Since there is some slight solubility of C in SiC, it is difficult to determine the Si/converted layer interface. Preliminary TEM results indicate a converted layer thickness of 120-300 Å depending on the growth time. Thus one half-three fourths of each profile may be inside the Si.

B. XPS Results

Binding Energies

From the XPS spectra obtained from both the unsputtered and sputtered converted layers and the sample containing the 5 x 10^{-6}m

thick β-SiC film, there were determined three different C/Si ratios: total C/total Si, carbide C/total Si and carbide C/carbide Si. The results of this research are presented in Table IV and figures 14-18, the latter of which are for the 150s sample and the β-SiC thin film. In all the unsputtered samples, C has two distinct binding energy peaks which represent (1) surface hydrocarbons with a binding energy (BE) of 284.9 eV ± 0.2 eV and (2) SiC with a BE of 282.7 eV ± 0.2 eV. Free C may also be present at or near the surface of the samples; however, it is difficult to determine this from the present data (see below). This combination of C sources is the reason for the values of the total C/total Si ratios being considerably in excess of 1:1 for all samples and for the similarity in values of this parameter for the 210, 180 and 150s samples.

The significant decrease in the carbide C/total Si ratios from those of the total C/total Si in the unsputtered samples is caused by the fact that only the carbide C peak is under consideration. However, the increase *in individual* values of the carbide C/carbide Si ratios of all the unsputtered samples relative to each of their companion values of the carbide C/total Si ratio stems from the fact that the values of total Si in the latter ratios are derived from both Si-C bonding and bonding between Si and an oxygen-containing component. The latter species is reasoned to be SiOH which formed as a result of exposure to air.

A perusal of the carbide C/carbide Si ratios of the unsputtered samples indicates that the ratio for the top surface of the 150s sample is close to the C/Si ratio of 0.96 which is that determined for the pure β-SiC film. This proximity in values correlates with the empirical results that the 150s conversion time provides the best final surface upon which to grow the β-SiC single crystal films. Longer and shorter conversion times indicate an excess or a deficit, respectively, in the amount of C relative to the β-SiC thin film. Since the solubility of C or Si in SiC is very small, the exact chemical meaning of having an excess or a deficit of carbide C relative to a 1:1 C/Si ratio is not known. However, it may be reasoned that the excess C in the 210 and 180s samples may be caused by either the presence of a free C component or a graphitic C component which is not resolvable from the carbide

TABLE IV. Carbon/Silicon Ratios Derived from XPS Data

Sample No. (Dep. time(s)	Total C/ Total Si (Unsputtered[a])	Carbide C/ Total Si (Unsputtered)	Carbide C/ Carbide Si (Unsputtered	Total C/ Total Si (Sputtered[b])	Carbide C/ Total Si (Sputtered	Carbide C/ Carbide Si (Sputtered
210	2.3	1.08	1.34	1.7	0.73	Study to be repeated as sputtering process punched through the converted layer into the Si substrate.
180	2.4	0.83	1.13	0.46	0.20	
150	2.3	0.73	0.90	0.65	0.36	
120	2.0	0.65	0.78	0.34	0.27	
β-SiC std. film	1.7	0.83	0.96	1.5	0.93	0.93

[a] Carbon peak shape has 2 components: hydrocarbon (BE = 284.9 eV ± 0.2 eV)
carbide (BE = 282.7 eV ± 0.2 eV)

[b] All 5 min. sputter except sample (3 min) = 10 min sputter.
Carbon peak shape has 1 major component: carbide (BE = 283.1 eV ± 0.3 eV)
Small amt. of residual hydrocarbon gives high BE tail

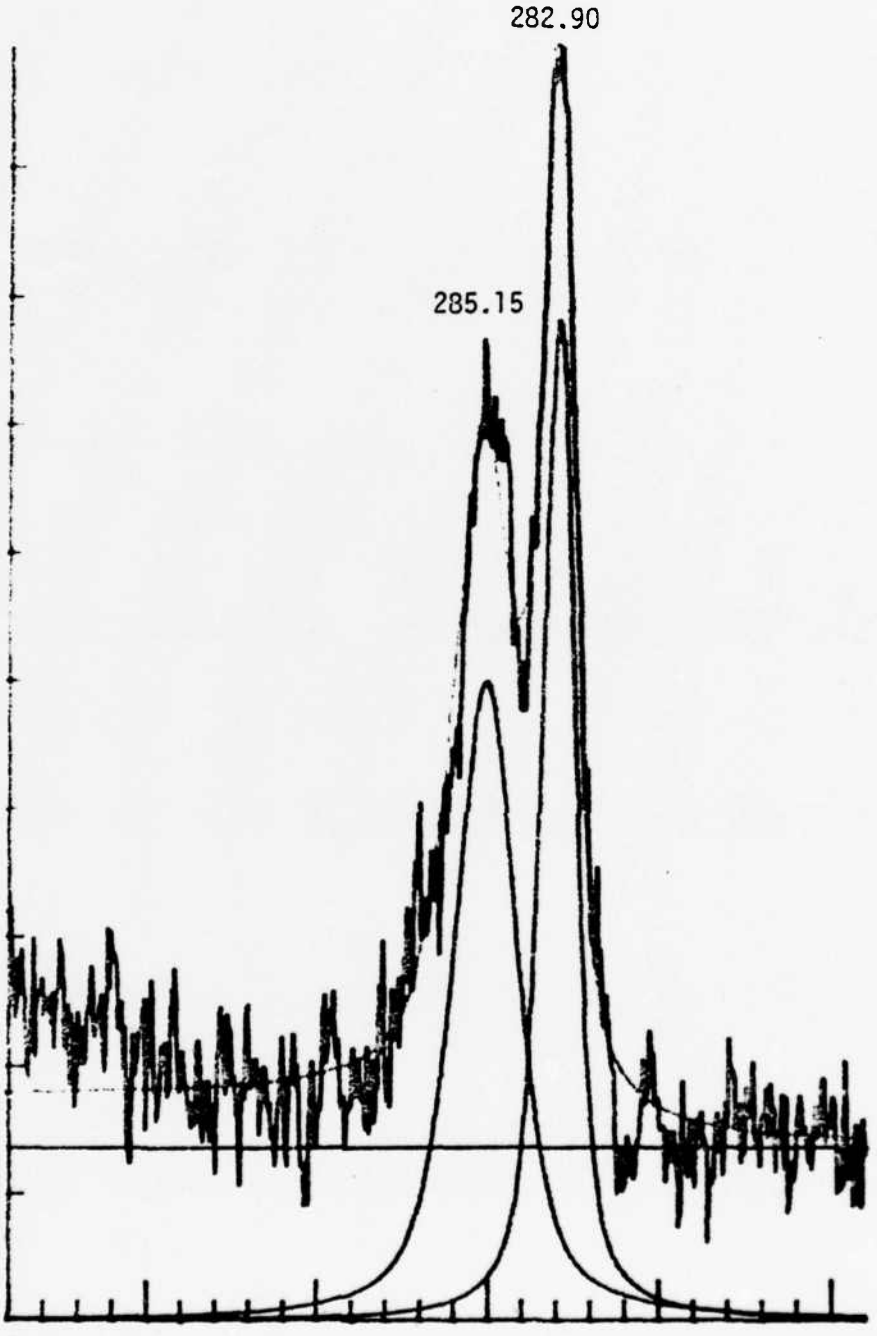

Figure 14. XPS C1s binding energy spectra derived from the unsputtered converted layer deposited on Si for 150s.

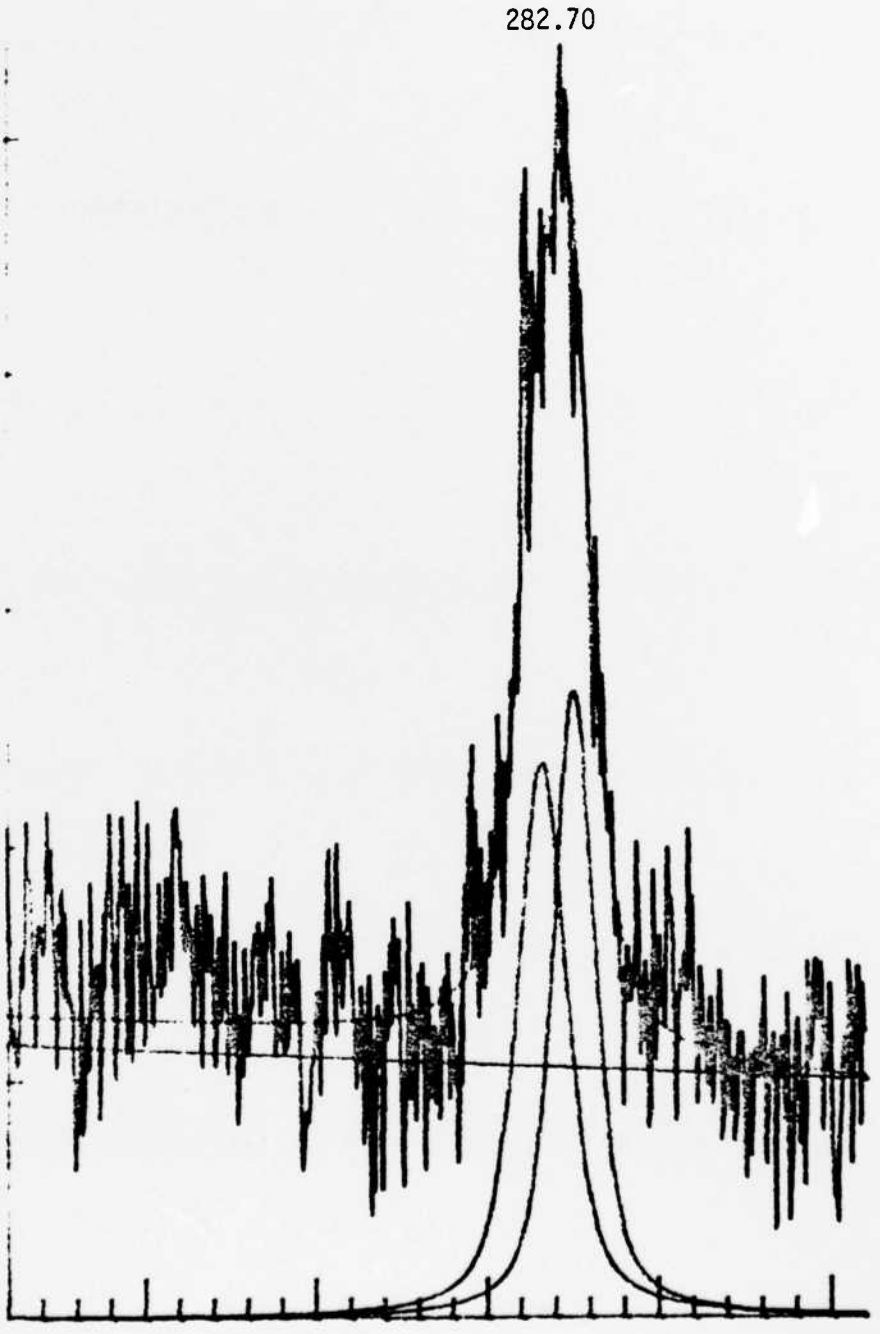

Figure 15. XPS C1s binding energy spectra derived from the sputtered (5 min) converted layer deposited on Si for 150s. Note the decrease in intensity of the hydrocarbon peak.

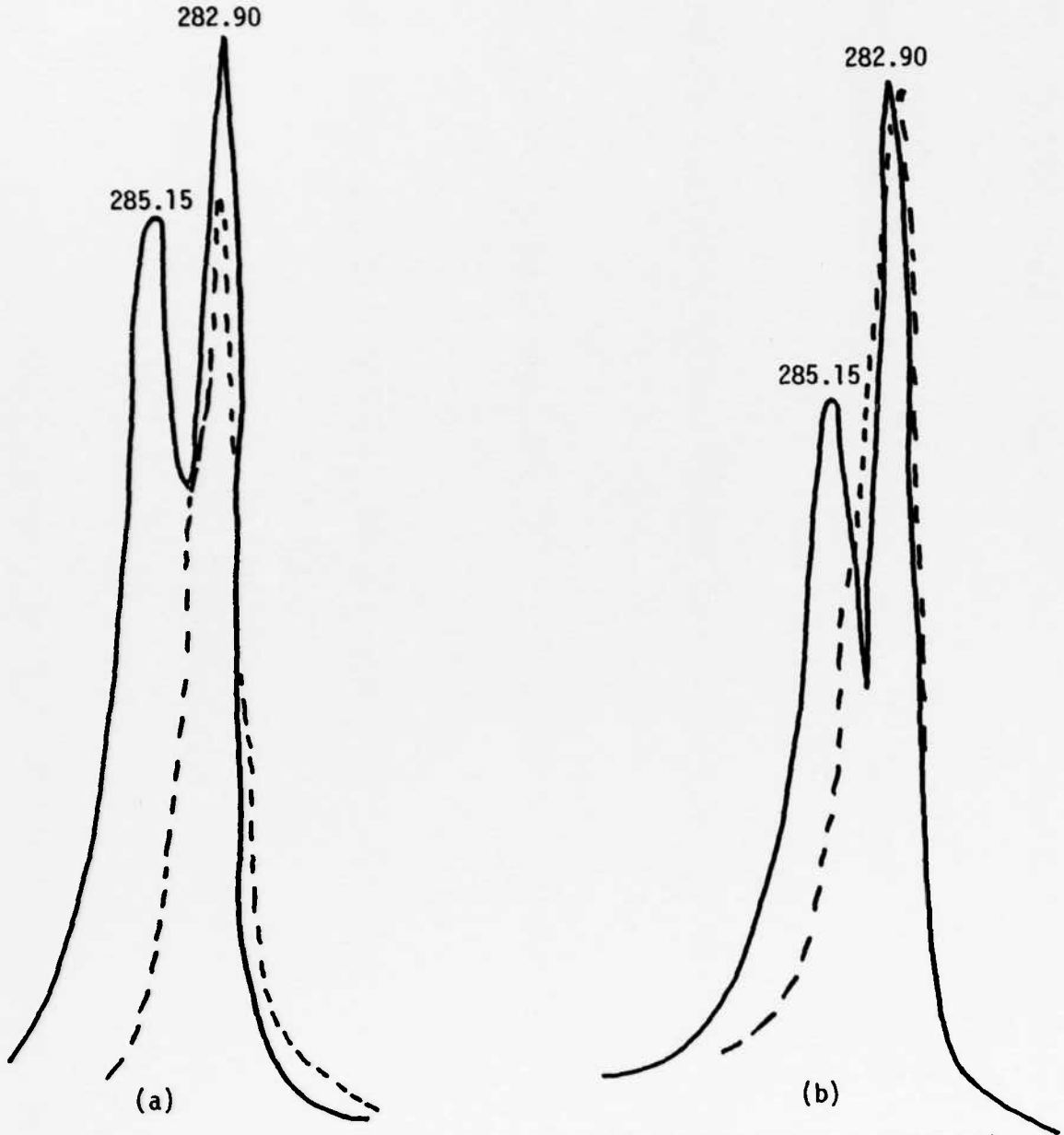

Figure 16. Composite graphs of the unsputtered (solid lines) and sputtered (dashed lines) 150s converted layer (a) and 5 x 10^{-6}m β-SiC thin film (b) which illustrate the dramatic decrease in the hydrocarbon peak with sputtering.

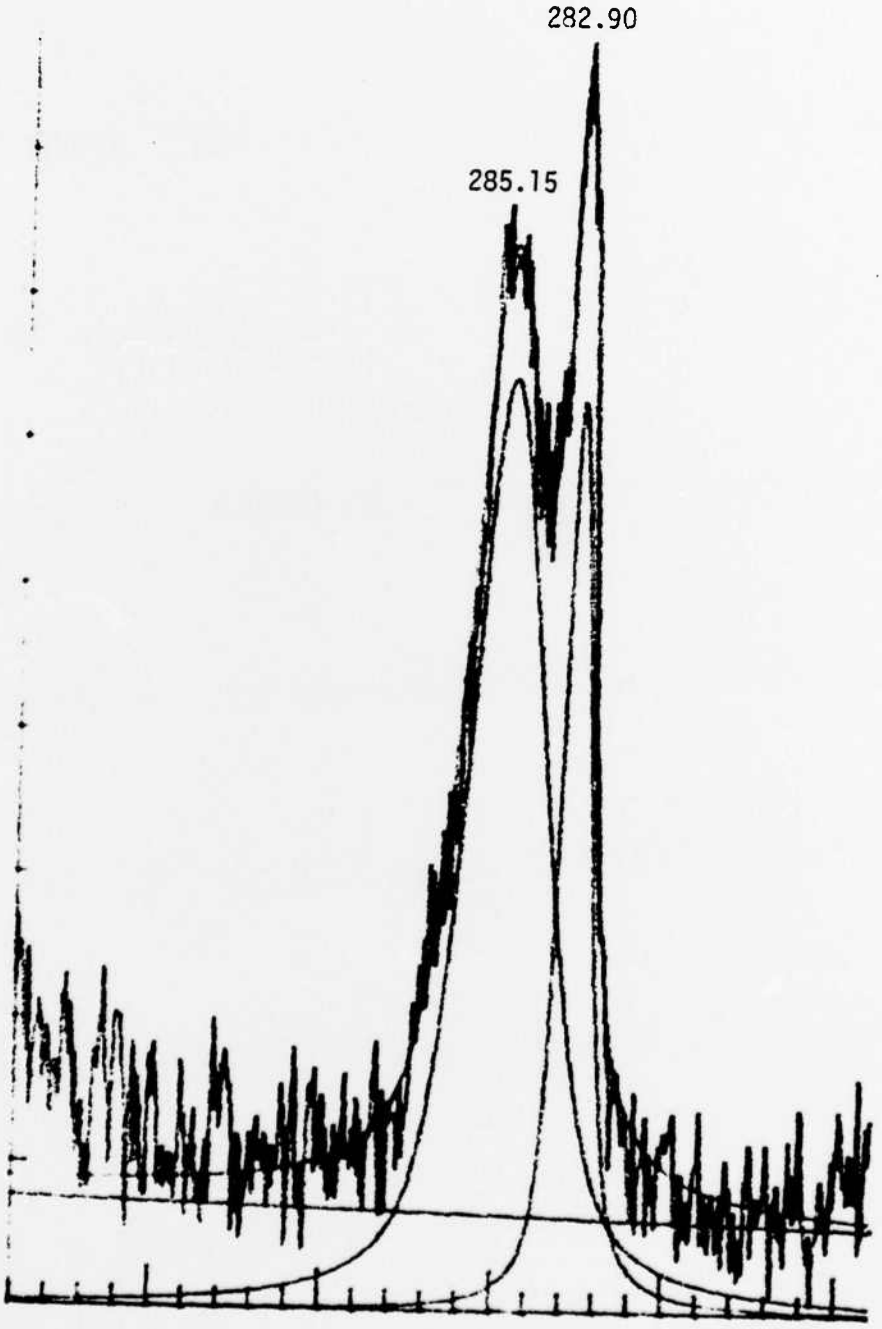

Figure 17. XPS C1s binding energy spectra derived from the unsputtered β-SiC thin film deposited on the 150s converted layer. The thickness of this film is approximately 5 x 10^{-6}m.

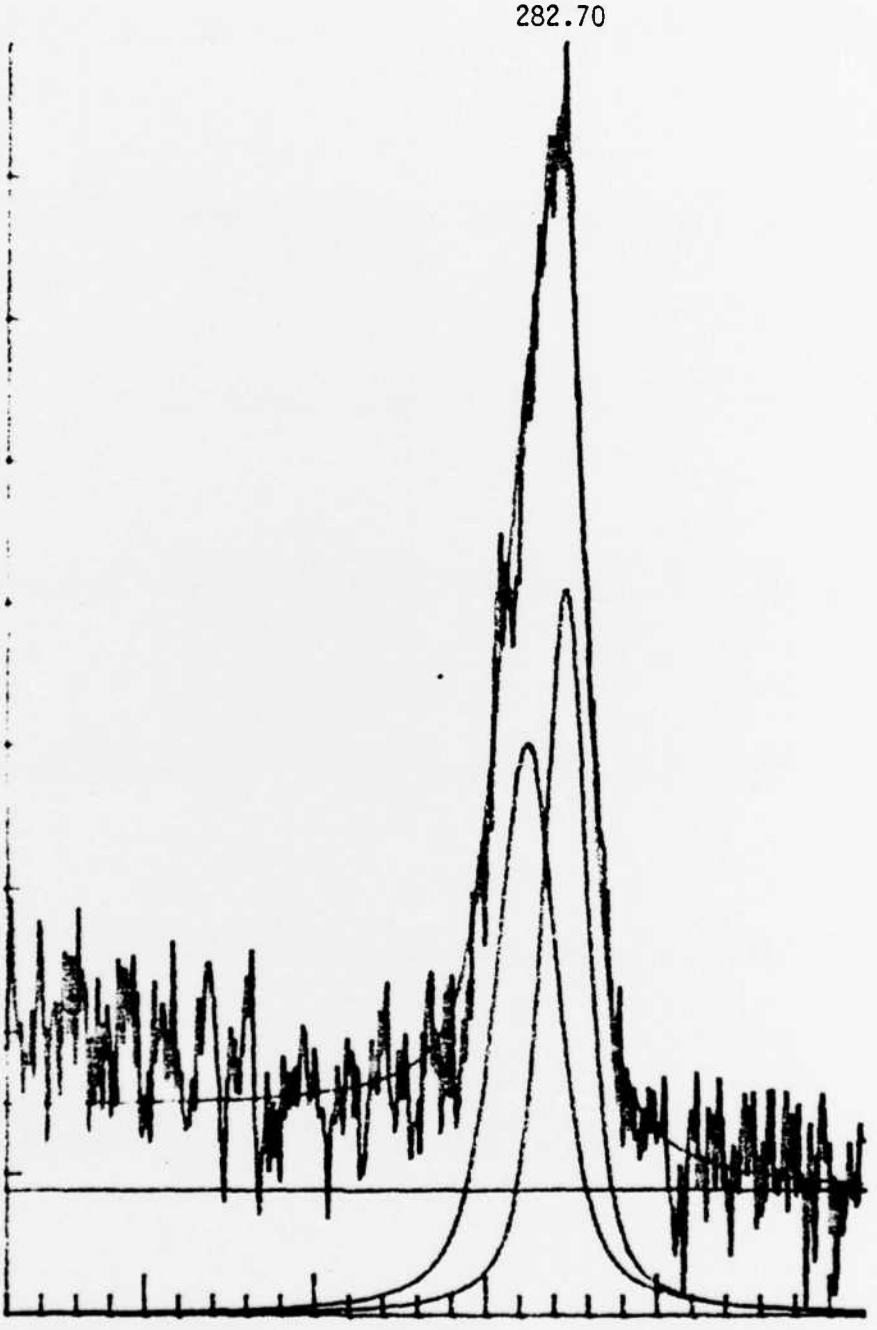

Figure 18. XPS C1s binding energy spectra derived from the sputtered (5 min) β-SiC thin film grown on the 150s converted layer. Note the sharp drop in the hydrocarbon peak.

component. The apparent deficit in carbide C in the 120s sample is probably caused by a small amount of sampling of the underlying surface of the Si substrate which, in fact, increases abnormally the Si count rate as occurred in the sputtered materials.

The decrease in the total C/total Si ratios of the sputtered samples having converted layers relative to the analogous unsputtered materials is due both to the elimination of the hydrocarbon component in the total C values and to the fact that the sputtering time was sufficiently long to penetrate the film such that the Si substrate contributed to the total Si values. The removal of the hydrocarbon is most evident in figure 16 which is a composite of the unsputtered and sputtered 150s sample. This figure reveals that after sputtering, one obtains a much reduced residual hydrocarbon peak that is shifted down in binding energy. This shift possibly signifies the presence of uncombined C which has a BE of 283.28 eV. Evidence for the beam penetration of the Si substrate may be seen by a comparison of the carbide C/total Si value of the 210s sample and the standard thin film sample whose respective ratios were not only essentially 1:1 but remained the same in the carbide C/carbide Si ratios. By contrast the carbide C peak remains the same in position and essentially the same in intensity, especially in the case of the standard sample. Finally, the value of 0.93 for the sputtered standard sample indicates that there is no apparent gross damage effects or preferntial sputtering which considerably distorts the stoichiometry of SiC.

The data for the carbide C/carbide Si ratios of the sputtered converted layer samples is not reported at this time because of the high Si content. The experiments are being repeated on new samples, and the data will be noted in the next report. Nevertheless it should be noted that based on known sputtering rates for Si for the equipment employed in this research, the SiC converted layers are all less than 10 nm thick.

Plasmon Data

The plasmon peaks which occur in XPS spectra from electron exitations resulting from inelastic scattering of the primary electron may also be used to complement and supplement the XPS information discussed above. A brief discussion of our findings in this area of study in the SiC materials is presented below.

The XPS spectra for the unsputtered 210 and 150s samples as well as the 5 x 10^{-6}m SiC thin film are shown in figures 19 and 24. There is very little difference among these spectra or between these representative spectra and those of the remaining samples in this study. A bulk SiC plasmon peak occurs at 122.5 eV or 23 eV higher than the Si_2 peak at 99.5 eV. In addition there is a minor surface SiC plasmon and/or a bulk Si plasmon at 116.5 eV or 17 eV above the Si_{2p} peak which occurs with only slight differences in all the unsputtered and sputtered samples (it is particularly evident on the 210s sample).

After sputtering the thinner converted layers, the SiC bulk plasmon virtually disappears as may be seen by a comparison of figures 22 and 23. The bulk Si plasmon at 116.5 eV appears as a consequence of sputtering through the converted layer sufficiently to sample the Si substrate. One may argue that this latter plasmon peak is a result of preferential sputtering of C. However this argument is weakened by the fact that a 300s Ar^+ sputter of the 210s film (figure 22) or the SiC standard thin film (figure 24) do not cause a surface depletion of C. This is also consistent with the quantitative C/Si ratios which show that after a 300 or 600s sputter, the surface is highly depleted in C. Finally, the decrease in prominence of the SiC bulk plasmon structure in the sputtered 210s sample (figure 22) relative to that of the unsputtered spectra (figure 19) is a result of Ar^+ beam damage, Ar^+ implantation, etc.

V. Future Research

Research for the next reporting period will include additional ion implantation and annealing studies with emphasis on the latter. Also, a wet/dry oxidation system will be established, our research on suitable contact materials (ohmic and Schottky) will be continued and additional XPS research on the converted layers will be conducted. Finally, in-situ doping of the as-grown layers and subsequent characterization will be initiated.

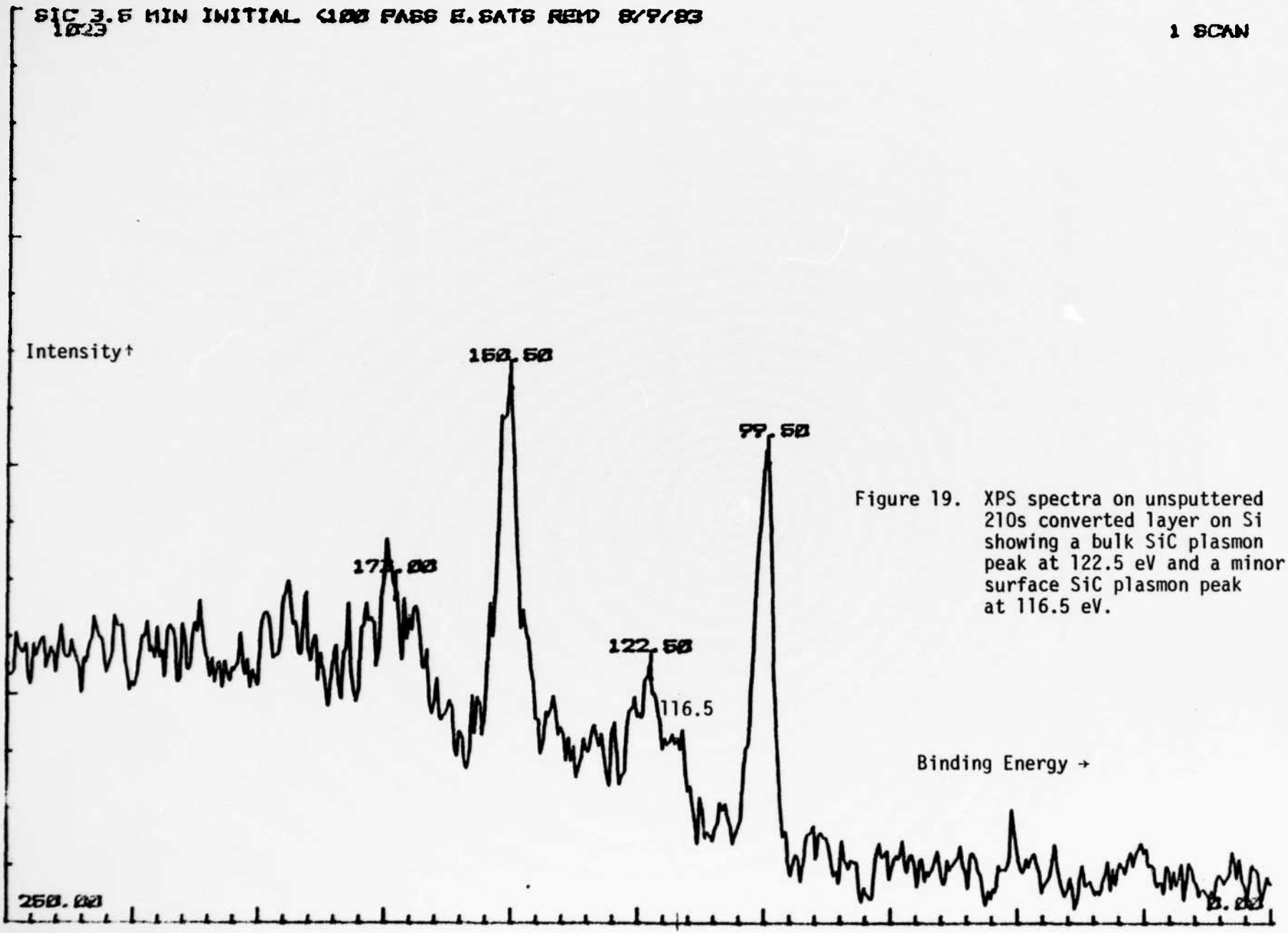

Figure 19. XPS spectra on unsputtered 210s converted layer on Si showing a bulk SiC plasmon peak at 122.5 eV and a minor surface SiC plasmon peak at 116.5 eV.

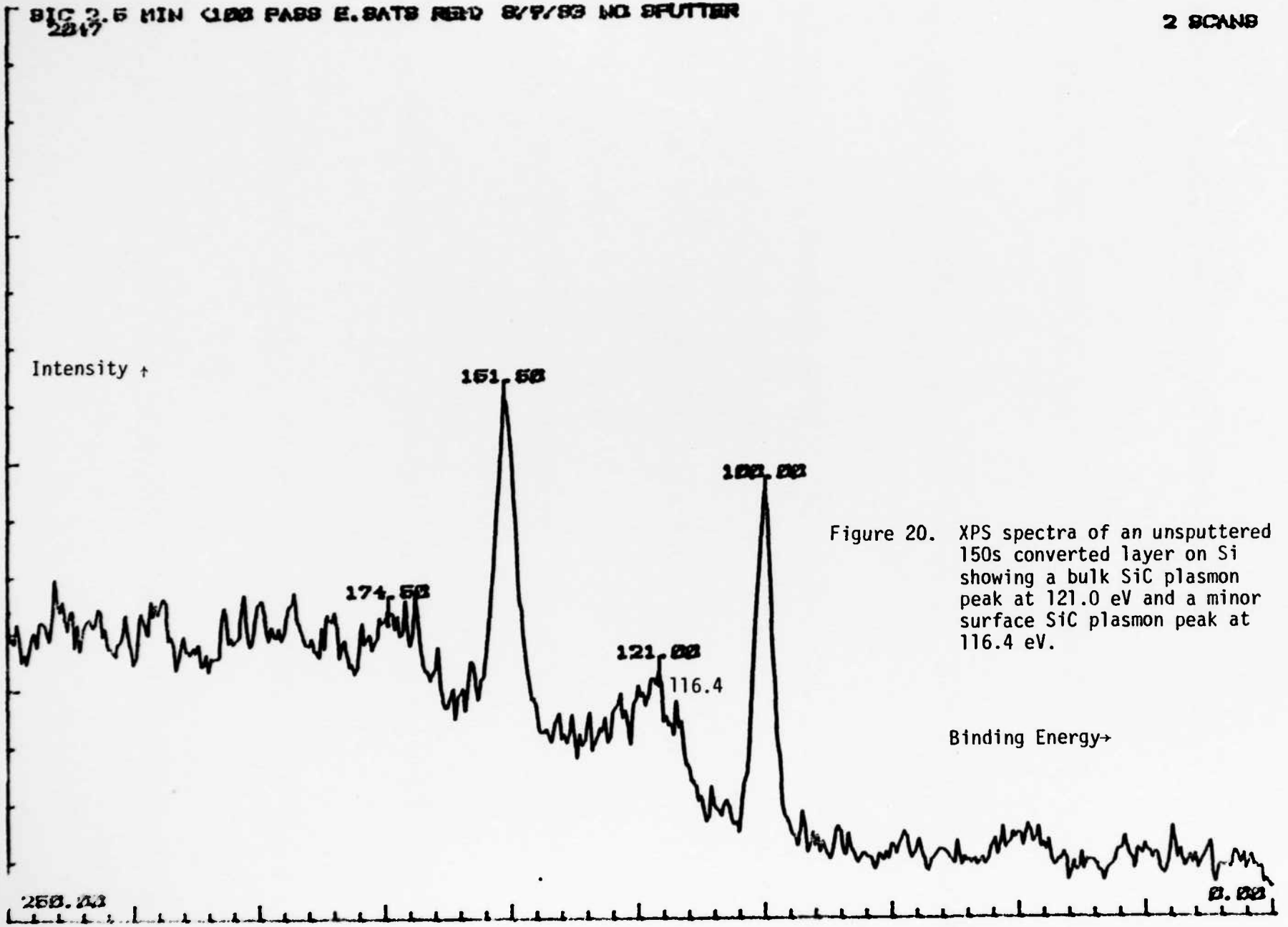

Figure 20. XPS spectra of an unsputtered 150s converted layer on Si showing a bulk SiC plasmon peak at 121.0 eV and a minor surface SiC plasmon peak at 116.4 eV.

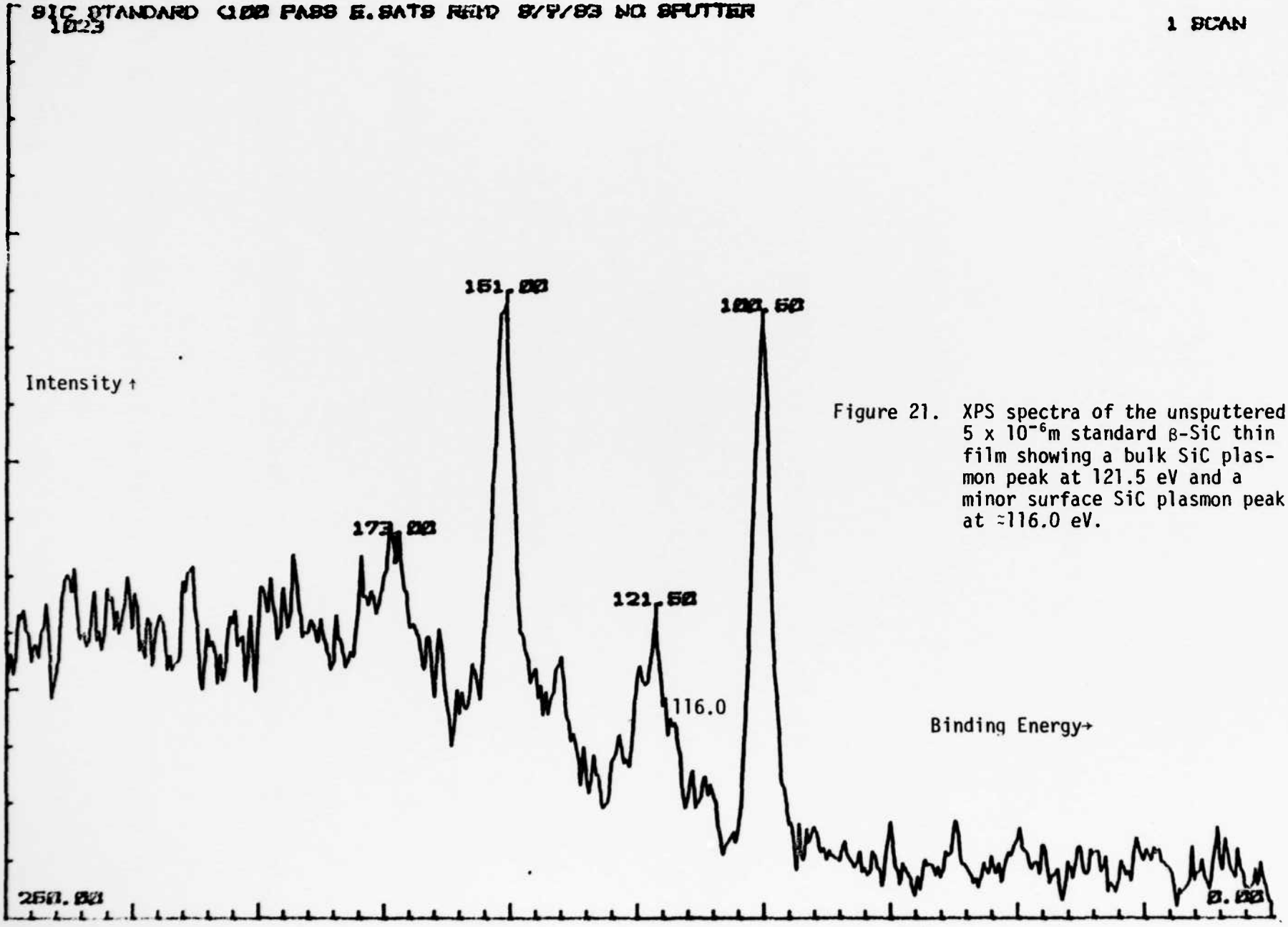

Figure 21. XPS spectra of the unsputtered 5×10^{-6}m standard β-SiC thin film showing a bulk SiC plasmon peak at 121.5 eV and a minor surface SiC plasmon peak at ≈116.0 eV.

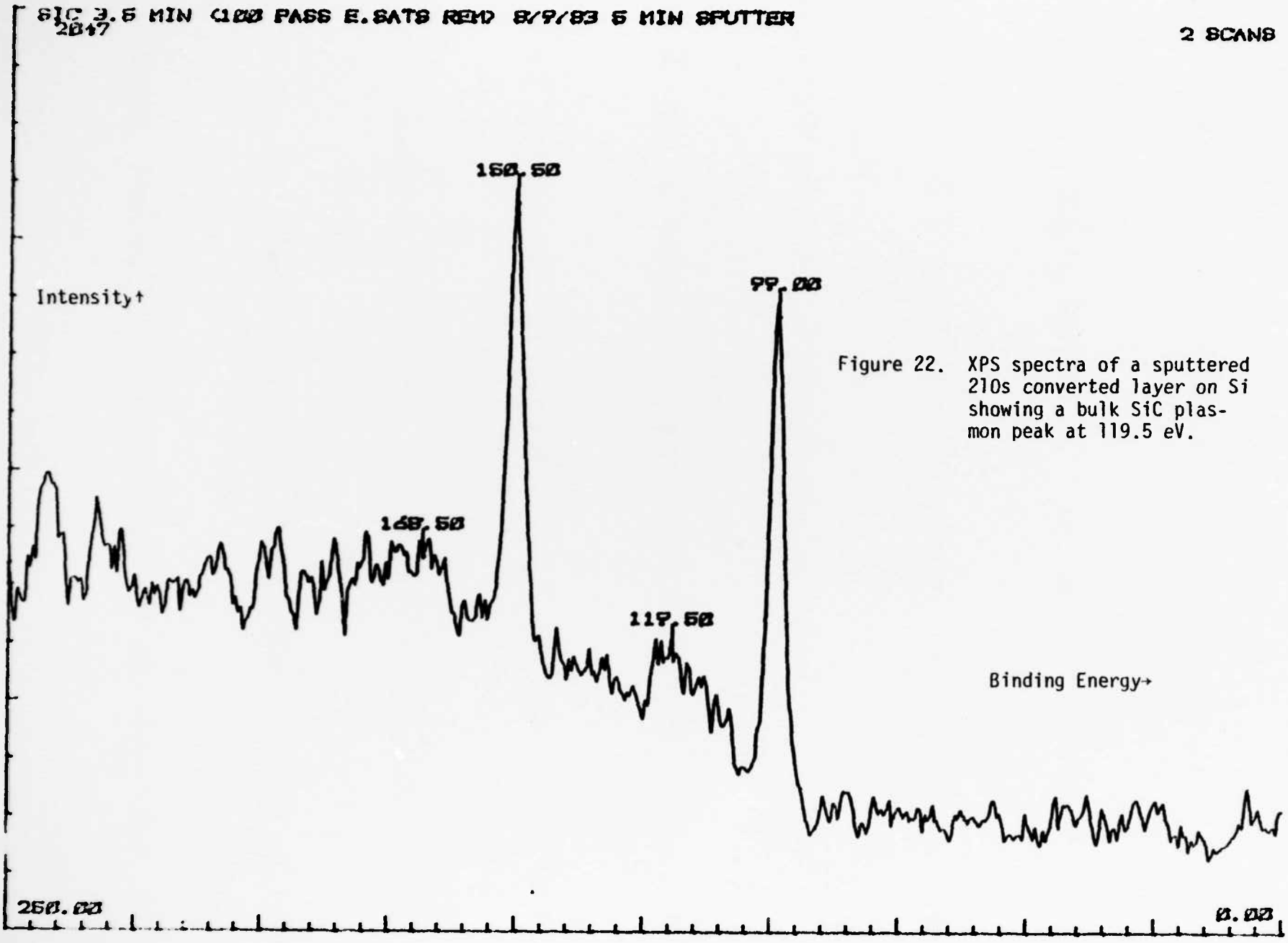

Figure 22. XPS spectra of a sputtered 210s converted layer on Si showing a bulk SiC plasmon peak at 119.5 eV.

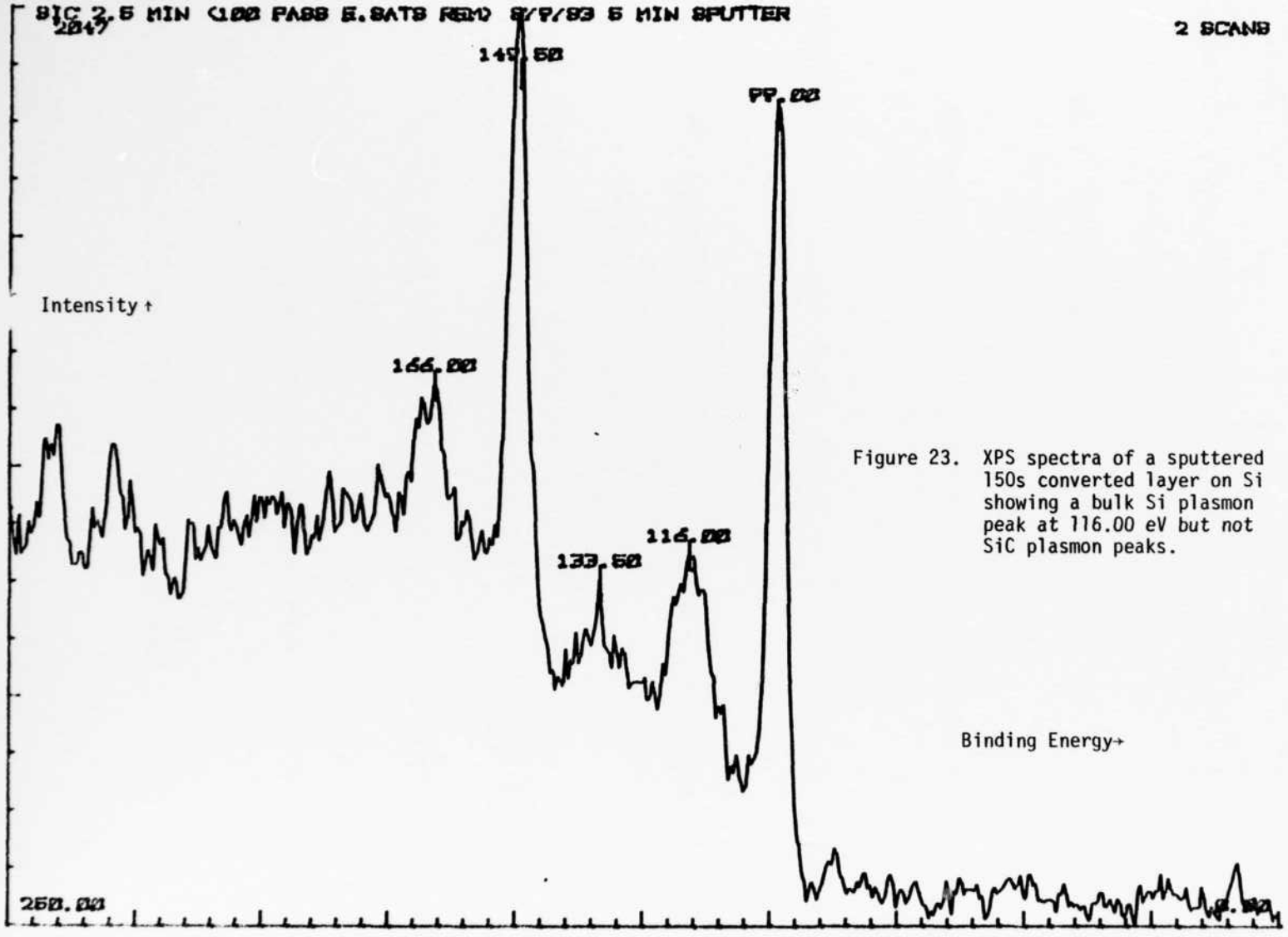

Figure 23. XPS spectra of a sputtered 150s converted layer on Si showing a bulk Si plasmon peak at 116.00 eV but not SiC plasmon peaks.

sputtered converted layers and the sample containing the 5 x 10

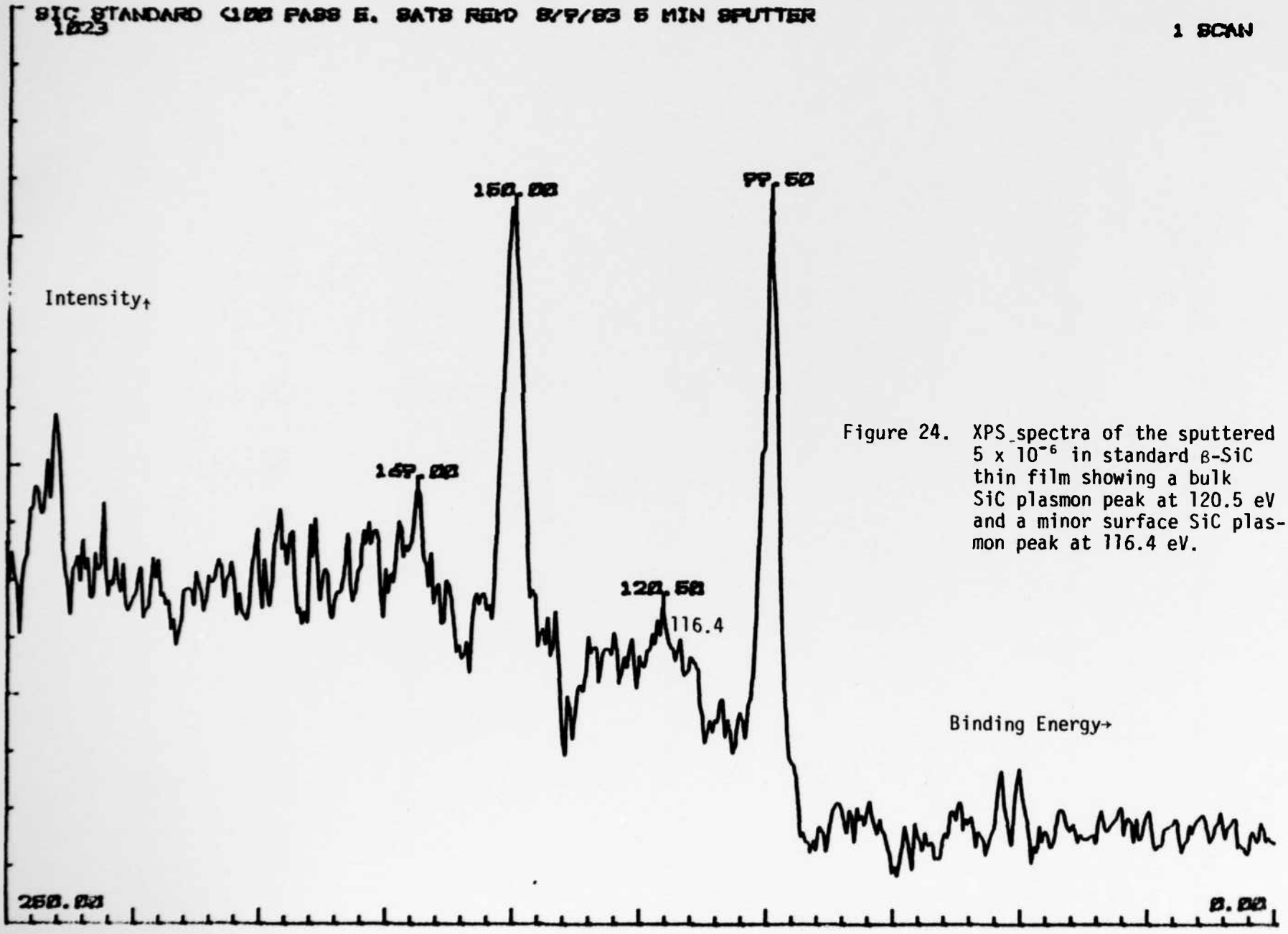

Figure 24. XPS spectra of the sputtered 5×10^{-6} in standard β-SiC thin film showing a bulk SiC plasmon peak at 120.5 eV and a minor surface SiC plasmon peak at 116.4 eV.

V. Bibliography

1. W. G. Spitzer, D. A. Kleinman, and C. J. Frosch, Phys. Rev., 113, 133 (1959).
2. H. Nakasima, T. Sugano, and H. Yanai, Jap. J. Appl. Phys., 5, 874 (1966).
3. J. Graul and E. Wagner, Appl. Phys. Lett., 21, 67 (1972).
4. M. Balog, A. Reisman, and M. Berkenblit, J. Elec. Mat., 9, 669 (1980).
5. J. Mercier and C. Roussel, in Third Int'l Con. on CVD, p. 426 (1972).
6. J. F. O'Hanlon, in A User's Guide to Vacuum Technology, John Wiley and Sons, New York, New York, pp. 21-2 (1980).
7. R. Glang, R. A. Holmwood, and J. A. Kurtz, in Handbook of Thin Film Technology, Ch. 2, Ed. by L. I. Maissel and R. Glang, McGraw-Hill Book Co., New York, New York, pp. 2-4 (1970).
8. I. H. Khan and R. N. Summergrad, Appl. Phys. Lett., 11, 12 (1967).
9. I. H. Khan, Mat. Res. Bull., 4, S285 (1969).
10. A. S. Brown and B. E. Watts, J. Appl. Cryst., 3, 172 (1970).
11. A. J. Learn and I. H. Khan, Thin Solid Films, 5, 145 (1970).
12. K. E. Haq and I. H. Khan, J. Vac. Sci. Technol., 7, 490 (1970).
13. C. J. Mogab and H. J. Leamy, J. Appl. Phys., 45, 1075 (1974).
14. L. Meyer and R. Gomer, Third Biannual Carbon Conference, Buffalo, New York (1957).
15. N. C. Tombs, J. J. Comer, and J. F. Fitzgerald, Solid State Elec., 8, 839 (1965).
16. R. I. Scace and G. A. Slack, in Silicon Carbide: A High Temperature Semiconductor, J. R. O'Conner and J. Smiltens (Eds.), Pergamon Press, New York, 1960, pp. 24-30.

DISTRIBUTION LIST - ANNUAL LETTER REPORT

CONTRACT N00014-82-K-0182

Address	No. of copies
Drs. Max Yoder/Ken Davis Office of Naval Research Electronics Program - Code 427 800 North Quincy Street Arlington, VA 22217	2
Ms. Nancy S. McHan ONR Resident Representative Georgia Institute of Technology 214 O'Keefe Building Atlanta, GA 30332	2
Director, Naval Research Laboratory ATTN: Code 2627 Washington, DC 20375	7
Defense Technical Information Center Bldg. 5 Cameron Station Alexandria, Virginia 22314	14
ONR Branch Office 536 South Clark Street Room 286 Chicago, IL 60605	2
Dr. J. Anthony Powell NASA Lewis 2100 Brookpark Rd. Cleveland, OH 44135	1
Dr. Ray Kaplan Code 6834 Department of the Navy Naval Research Laboratory Washington, DC 20375	1

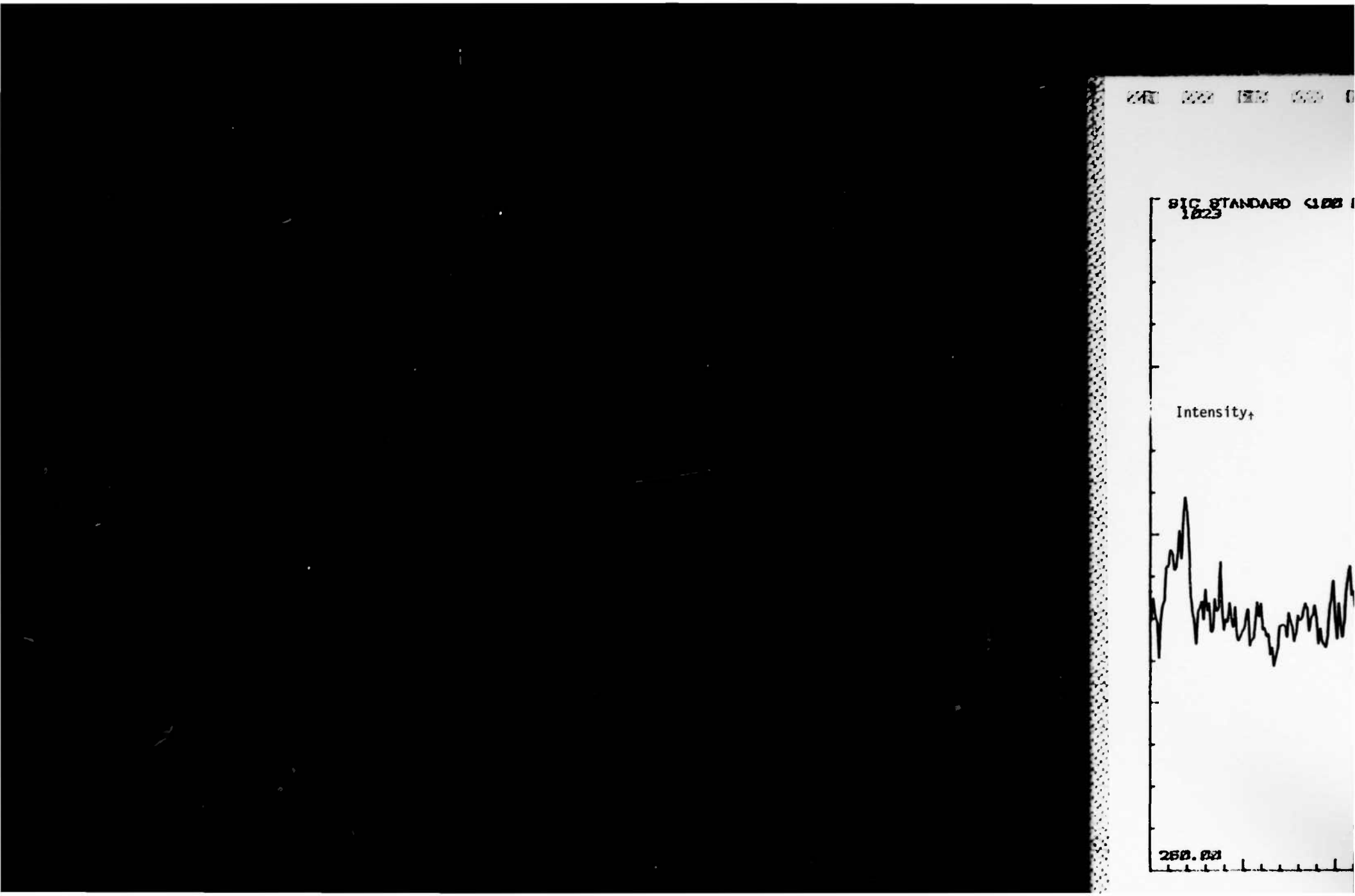
SIC STANDARD
1023
Intensity
250.00